Electronic Supplementary Material (ESI) for Dalton Transactions.

Electronic Supplementary Information (ESI) for:

Assembly, Disassembly and Reassembly : a "Top-Down" Synthetic Strategy towards Hybrid, Mixed-Metal {$Mo_{10}Co_6$} POM Clusters

Colm Healy,[a,b] Friedrich W. Steuber,[a] Paul Wix,[a] Lauren K. Macreadie,[a,c] Amal Cherian Kathalikkattil[a] and Wolfgang Schmitt*[a]

[a] School of Chemistry and CRANN, Trinity College Dublin, College Green, Dublin 2, Ireland

[b] MacDiarmid Institute for Advanced Materials and Nanotechnology, School of Physical and Chemical Sciences, University of Canterbury, Private Bag 4800, Christchurch 8041, New Zealand

[c] CSIRO Manufacturing, Bayview Ave, Clayton, VIC 3168, Australia

Contents: **Page:**

1) Synthetic Procedures

Lindqvist Hexamolybdate, $[TBA]_2[Mo_6O_{19}]$

Lindqvist hexamolybdate was prepared by a literature procedure.[1] Sodium molybdate (2.5 g, 10.3 mmol) was dissolved in 10 ml of water and acidified drop-wise with hydrochloric acid (35 %, 1.75 ml). A solution of TBA bromide (1.2 g, 3.75 mmol in 2 ml water) was added, producing a white precipitate. The slurry was refluxed overnight, turning yellow. The resulting yellow solid was isolated by filtration and washed with water and diethyl ether before air-drying for one hour. The solid was then purified through recrystallisation from boiling acetone (*c.* 100 ml) and storing at −20 °C overnight to yield large, yellow crystals. The crystals were isolated by filtration, washed with diethyl ether and air dried. Yield: 1.62 g, 69 %. FT-IR υ_{max} (cm^{-1}): 2962 (w), 2873 (w), 1468 (m), 951 (Mo=O) (s), 789 (Mo-O bridging) (s).

Adamantylphosphonic Acid

Adamantylphosphonic acid was prepared by a modification of literature procedure for other tertiary phosphonic acids.[2] Solid 1-bromoadamantane (5.4 g, 25 mmol) and aluminium trichloride (3.33 g, 25 mmol) were combined at 0 °C, followed by slow addition of excess phosphorus trichloride (10 ml) at 0 °C. After standing at room temperature overnight, the solid was dispersed in chloroform (100 ml) and subsequently poured over a mixture of ice (100 g) and hydrochloric acid (35 %, 50 ml) and stirred vigorously for *c.* 15 minutes, adding more ice as required. The chloroform layer was allowed to separate, and the aqueous layer extracted again with chloroform. The combined chloroform solutions were dried using $MgSO_4$ and evaporated under reduced pressure. Without further purification, the resulting solid was added to a concentrated aqueous KOH (50 ml) solution at 0 °C before refluxing overnight. The solution was subsequently neutralised with ice-cold HCl at 0 °C, resulting in a white precipitate that was washed with copious amounts of water and dried under vacuum. Yield: 3.5 g, 65 %.

General Synthetic Procedure

$[TBA]_2[Mo_6O_{19}]$ (0.068 g, 0.05 mmol), a cobalt (II) carboxylate salt (0.25 mmol), a phosphonic acid (0.25 mmol) and tetrabutylammonium bromide (0.161 g, 0.5 mmol) were combined in acetonitrile (25 ml). Alternatively, cobalt (II) nitrate hexahydrate (0.073 g, 0.25 mmol) and a carboxylic acid (0.5 mmol) could be used. Pyridine or picoline (0.5 mmol) was subsequently added. The solution was stirred at room temperature for four hours with the appearance of a dark purple colour. The purple solution was filtered to remove any solid material, and the solvent was allowed to evaporate slowly until pink-purple crystals suitable for X-ray diffraction analysis formed (usually 1–2 weeks). The crystals were isolated by filtration, washed with diethyl ether and air dried. In some cases, the crystals were contaminated by an unidentified, insoluble dark blue solid; in these instances the solids were re-dissolved in acetonitrile, the blue solid removed by filtration, and the crystallisation procedure repeated.

$[TBA]_2[Mo^{VI}_{10}Co^{II}_6O_{12}(\mu\text{-}O)_{14}(\mu_3\text{-}O)_4(\mathit{t}BuPO_3)_6(MeCOO)_2(py)_2(H_2O)_6]\cdot4(MeCN)$, 1

Yield: 0.076 g, 68.8% based on Mo. FT-IR (ATR) υ_{max} (cm^{-1}): 3460 (w), 3425 (w), 3147 (b), 2964 (w) (C-H), 2873 (w) (C-H), 1644 (w), 1600 (w), 1568 (ν_{sym}) (m), 1479 (m), 1445 (m), 1417 (sh) (ν_{asym}) (Δ = 151), 1396 (w), 1097 (s) (P-O), 975 (s) (P-O), 956 (s) (P-O), 891 (s) (Mo=O), 771 (s), 699 (s) (Mo-O). CHN Analysis for $Mo_{10}Co_6P_6O_{58}N_8C_{78}H_{166}$; Expected C% 25.72, H% 4.59, N% 3.08; Found C% 26.45, H% 4.35, N% 2.85. UV-Vis λ_{max}/nm (ε_{max}/M^{-1} cm^{-1}): 560 (341). MALDI-MS for $Mo_{10}Co_6P_6O_{53}N_1C_{44}H_{98}$ (loss of 1 TBA, 2 py, 5 H_2O) calculated *m/z* 2900.00, observed *m/z* 2900.01.

$[TBA]_2[Mo^{VI}_{10}Co^{II}_6O_{12}(\mu\text{-}O)_{14}(\mu_3\text{-}O)_4(\mathit{t}BuPO_3)_6(MeCOO)_2(pic)_4(H_2O)_6]\cdot4.4(MeCN)$, 2

Yield 0.043 g, 51.7% based on Mo. FT-IR (ATR) υ_{max} (cm^{-1}): 3469 (w), 3432 (w), 3180 (b), 2963 (w) (C-H), 2872 (w) (C-H), 1634 (w), 1596 (m), 1544 (ν_{sym}) (m), 1479 (m), 1407 (m) (ν_{asym}) (Δ = 137), 1363 (w), 1096 (s) (P-O), 974 (s) (P-O), 939 (s) (P-O), 8862(s) (Mo=O), 850 (s), 832 (s), 770 (s), 700 (s) (Mo-O). MALDI-MS for $Mo_{10}Co_6P_6O_{53}N_1C_{44}H_{98}$ (loss of 1 TBA, 4 pic, 5 H_2O) calculated *m/z* 2900.00, observed *m/z* 2900.01.

$[TBA]_2[Mo^{VI}_{10}Co^{II}_6O_{12}(\mu\text{-}O)_{14}(\mu_3\text{-}O)_4(\mathit{t}BuPO_3)_6(PhCOO)_2(py)_2(H_2O)_6]$, 3

Yield: 0.060 g, 55.5% based on Mo. FT-IR (ATR) υ_{max} (cm^{-1}): 3487 (w), 3441 (w), 3240 (b), 2970 (w) (C-H), 2869 (w) (C-H), 1738 (m), 1602 (m), 1564 (ν_{sym}) (m), 1538 (m), 1479 (m), 1405 (m) (ν_{asym}) (Δ = 159), 1215 (w), 1096 (s) (P-O), 973 (s) (P-O), 938 (s) (P-O), 890 (s) (Mo=O), 768 (s), 707 (s) (Mo-O). MALDI-MS for $Mo_{10}Co_6P_6O_{52}N_1C_{54}H_{100}$ (loss of 1 TBA, 2 py, 6 H_2O) calculated *m/z* 3094.02, observed *m/z* 3094.16.

$[TBA]_2[Mo^{VI}_{10}Co^{II}_6O_{12}(\mu\text{-}O)_{14}(\mu_3\text{-}O)_4(\mathit{t}BuPO_3)_6(BzCOO)_2(py)_2(H_2O)_6]\cdot3.5(MeCN)$, 4

Yield: 0.045 g, 39.7% based on Mo. FT-IR (ATR) υ_{max} (cm^{-1}): 3469 (w), 3432 (w), 3171 (b), 2964 (w) (C-H), 2874 (w) (C-H), 1639 (w), 1602 (m), 1560 (ν_{sym}) (m), 1478 (m), 1396 (m) (ν_{asym}) (Δ = 164), 1293 (w), 1096 (s) (P-O), 975 (s) (P-O), 953 (s) (P-O), 891 (s) (Mo=O), 850 (s), 823 (s), 770 (s), 700 (s) (Mo-O). CHN Analysis for $Mo_{10}Co_6P_6O_{58}N_4C_{82}H_{162}$; Expected C% 27.12, H% 4.49, N% 1.54; Found C% 27.04, H% 4.41, N% 1.26. MALDI-MS for $Mo_{10}Co_6P_6O_{52}N_1C_{56}H_{104}$ (loss of 1 TBA, 2 py, 6 H_2O) calculated *m/z* 3122.05, observed *m/z* 3122.05.

$[TBA]_2[Mo^{VI}_{10}Co^{II}_6O_{12}(\mu\text{-}O)_{14}(\mu_3\text{-}O)_4(\mathit{t}BuPO_3)_6(AdCOO)_2(py)_2(H_2O)_6]$, 5

Yield 0.034 g, 40.3% based on Mo. FT-IR (ATR) υ_{max} (cm^{-1}): 3478 (w), 3155 (b), 2903 (w) (C-H), 1640 (w), 1602 (m), 1535 (ν_{sym}) (m), 1479 (m), 1445 (m), 1395 (sh) (ν_{asym}) (Δ = 140), 1312 (w), 1097 (s) (P-O), 973 (s) (P-O), 947 (s) (P-O), 912 (s), 890 (s) (Mo=O), 850 (s), 826 (s), 770 (s), 699 (s) (Mo-O). CHN Analysis for $Mo_{10}Co_6P_6O_{58}N_4C_{88}H_{178}$; Expected C% 28.41, H% 4.82, N% 1.50; Found C% 28.69, H% 4.71, N% 1.45. MALDI-MS for $Mo_{10}Co_6P_6O_{50}C_{35}H_{69}$ (loss of 2 TBA, 1 AdCOO, 2 py, 6 H_2O) calculated *m/z* 2790.79, observed *m/z* 2790.82.

$[TBA]_2[Mo^{VI}_{10}Co^{II}_6O_{12}(\mu\text{-}O)_{14}(\mu_3\text{-}O)_4(AdPO_3)_6(MeCOO)_2(py)_2(H_2O)_6]\cdot 9.5(MeCN)$, 6

Yield 0.016 g, 17.3% based on Mo. FT-IR (ATR) υ_{max} (cm^{-1}): 3189 (b), 2903 (w) (C-H), 2850 (w) (C-H), 1604 (m), 1562 (ν_{sym}) (m), 1486 (m), 1446 (m), 1383 (w) (ν_{asym}) (Δ = 179), 1098 (s) (P-O), 968 (s) (P-O), 948 (s) (P-O), 886 (s) (Mo=O), 850 (s), 823 (s), 765 (s), 699 (s) (Mo-O). MALDI-MS for $Mo_{10}Co_6P_6O_{56}N_1C_{80}H_{140}$ (loss of 1 TBA, 2 py, 2 H_2O) calculated *m/z* 3511.32, observed *m/z* 3511.34.

$[TBA]_2[Mo^{VI}_{10}Co^{II}_6O_{12}(\mu\text{-}O)_{14}(\mu_3\text{-}O)_4(AdPO_3)_6(PhCOO)_2(py)_2(H_2O)_6]\cdot 2(MeCN)$, 7

Yield 0.012 g, 9.6% based on Mo. FT-IR (ATR) υ_{max} (cm^{-1}): 3456 (w), 3167 (b), 2903 (w) (C-H), 2850 (w) (C-H), 1640 (w), 1601 (m), 1535 (ν_{sym}) (m), 1484 (m), 1446 (m), 1407 (m) (ν_{asym}) (Δ = 128), 1097 (s) (P-O), 970 (s) (P-O), 952 (s) (P-O), 887 (s) (Mo=O), 827 (s), 768 (s), 697 (s) (Mo-O). CHN Analysis for $Mo_{10}Co_6P_6O_{58}N_4C_{116}H_{194}$; Expected C% 34.21, H% 4.80, N% 1.37; Found C% 34.04, H% 4.58, N% 1.53. MALDI-MS for $Mo_{10}Co_6P_6O_{56}N_1C_{90}H_{144}$ (loss of 1 TBA, 2 py, 2 H_2O) calculated *m/z* 3634.35, observed *m/z* 3634.43.

$[TBA]_2[Mo^{VI}_{10}Co^{II}_6O_{12}(\mu\text{-}O)_{14}(\mu_3\text{-}O)_4(AdPO_3)_6(BzCOO)_2(py)_3(H_2O)_6]\cdot 5(MeCN)$, 8

Yield 0.027 g, 20.5% based on Mo. FT-IR (ATR) υ_{max} (cm^{-1}): 3431 (w), 3167 (b), 2903 (w) (C-H), 2850 (w) (C-H), 1567 (ν_{sym}) (m), 1485 (m), 1446 (m), 1407 (m) (ν_{asym}) (Δ = 160), 1098 (s) (P-O), 978 (s) (P-O), 950 (s) (P-O), 888 (s) (Mo=O), 851 (s), 824 (s), 771 (s), 701 (s) (Mo-O). MALDI-MS for $Mo_{10}Co_6P_6O_{52}N_1C_{92}H_{140}$ (loss of 1 TBA, 2 py, 5 H_2O) calculated *m/z* 3591.34, observed *m/z* 3591.37.

$[TBA]_2[Mo^{VI}_{10}Co^{II}_6O_{12}(\mu\text{-}O)_{14}(\mu_3\text{-}O)_4(AdPO_3)_6(AdCOO)_2(py)_2(H_2O)_6]\cdot 6(MeCN)$, 9

Yield 0.031 g, 23.3% based on Mo. FT-IR (ATR) υ_{max} (cm^{-1}): 3181 (b), 2903 (w) (C-H), 1602 (w), 1534 (ν_{sym}) (m), 1480 (m), 1446 (m), 1421 (m) (ν_{asym}) (Δ = 113), 1097 (s) (P-O), 973 (s) (P-O), 947 (s) (P-O), 890 (s) (Mo=O), 851 (s), 829 (s), 771 (s), 699 (s) (Mo-O). MALDI-MS for $Mo_{10}Co_6P_6O_{52}N_1C_{98}H_{156}$ (loss of 1 TBA, 2 py, 6 H_2O) calculated *m/z* 3678.48, observed *m/z* 3678.47.

$[TBA]_2[Mo^{VI}_{10}Co^{II}_6O_{12}(\mu\text{-}O)_{14}(\mu_3\text{-}O)_4(t\text{BuPO}_3)_6(PDA)(py)_2(H_2O)_6]\cdot 7.5(MeCN)$, 10

Yield 0.022 g, 19.0% based on Mo. FT-IR (ATR) υ_{max} (cm^{-1}): 3435 (w), 3159 (b), 2964 (w) (C-H), 2872 (w) (C-H), 1566 (m) (ν_{sym}), 1477 (m), 1446 (m), 1401 (m) (ν_{asym}) (Δ = 165), 1096 (s) (P-O), 974 (s) (P-O), 949 (s) (P-O), 890 (s) (Mo=O), 853 (s), 825 (s), 769 (s), 700 (s) (Mo-O). CHN Analysis for $Mo_{10}Co_6P_6O_{58}N_8C_{92}H_{166}$; Expected C% 25.69, H% 4.42, N% 1.57, Found C% 25.46, H% 4.30, N% 1.28.

2) Additional Images of Compound 1

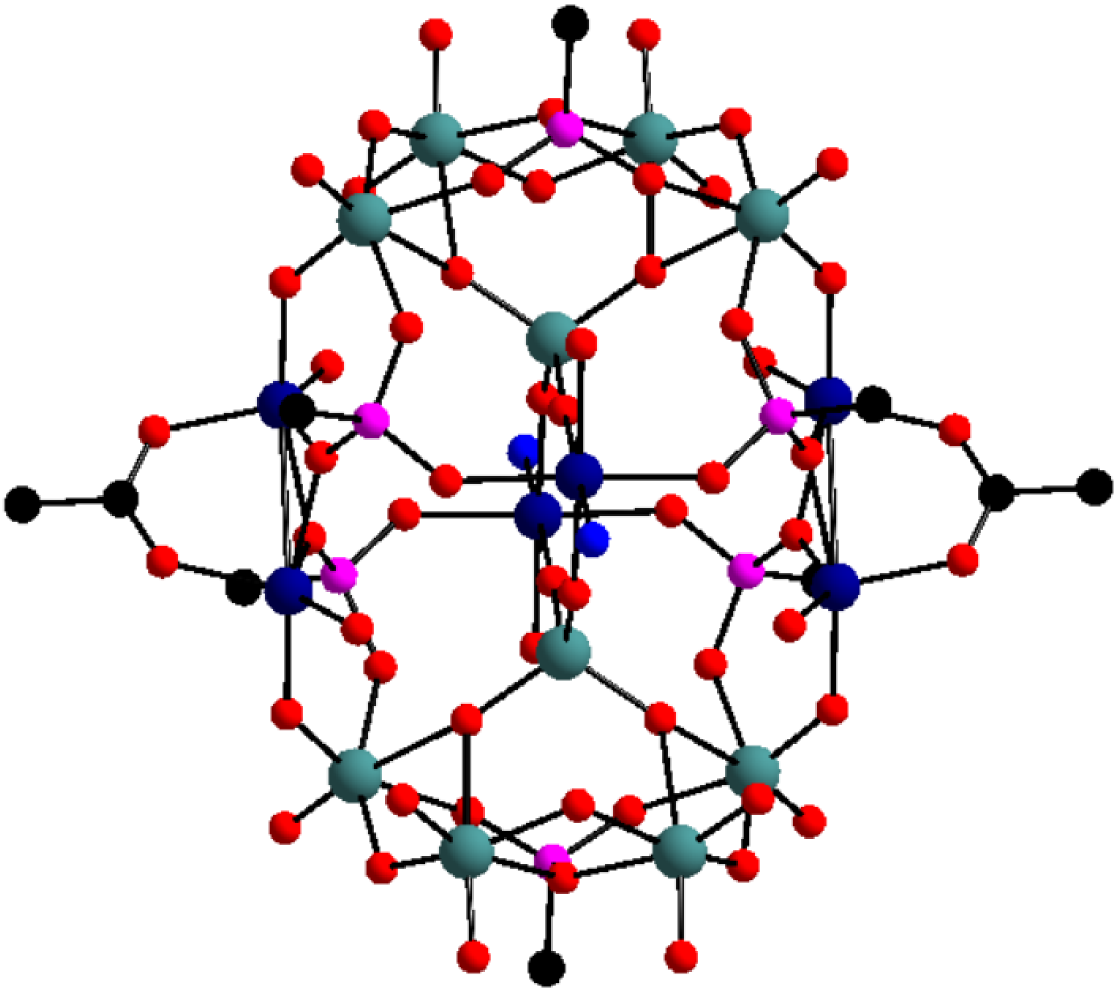

Figure S1. Structure of the anionic cluster in **1** in ball-and-stick representation, front view. *Tert*-butyl and pyridyl groups are reduced to a single C or N atom, respectively. H atoms are omitted. Colour Scheme: Mo teal, Co dark blue, P pink, O red, N blue, C black.

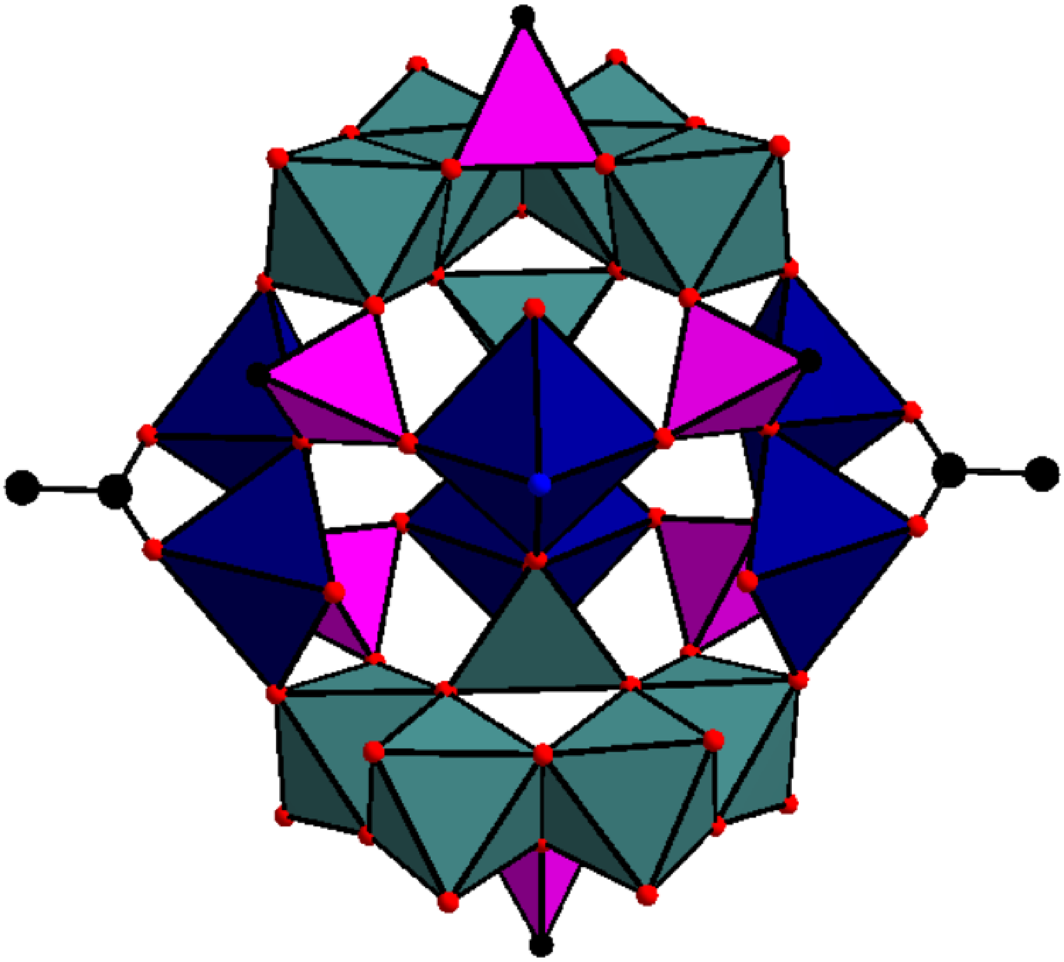

Figure S2. Structure of the anionic cluster in **1** in polyhedral representation, front view. *Tert*-butyl and pyridyl groups are reduced to a single C or N atom, respectively. H atoms are omitted. Colour Scheme: Mo teal, Co dark blue, P pink, O red, N blue, C black.

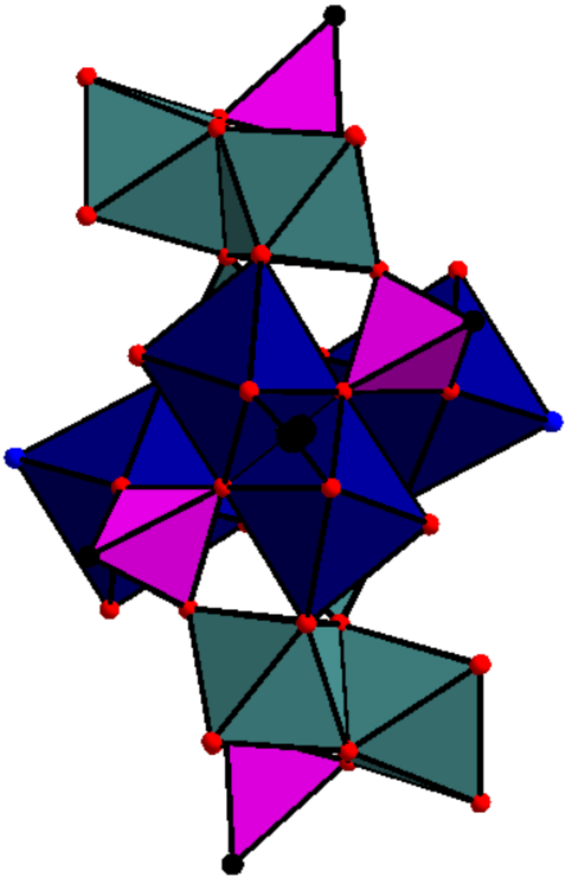

Figure S3. Structure of the anionic cluster in **1** in polyhedral representation, side view. *Tert*-butyl and pyridyl groups are reduced to a single C or N atom, respectively. H atoms are omitted. Colour Scheme: Mo teal, Co dark blue, P pink, O red, N blue, C black.

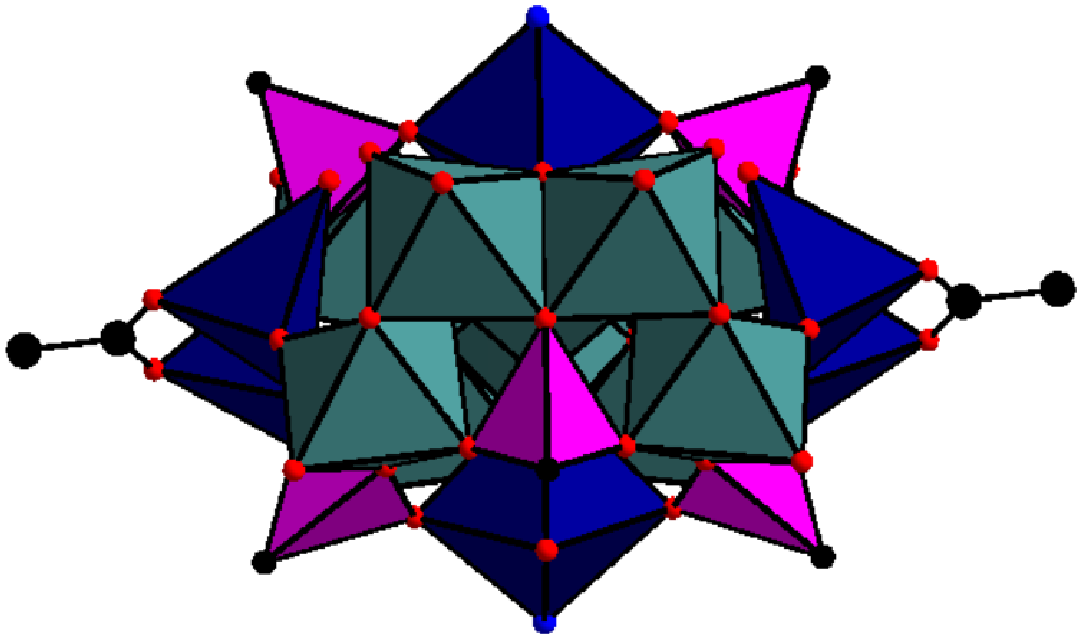

Figure S4. Structure of the anionic cluster in **1** in polyhedral representation, top view. *Tert*-butyl and pyridyl groups are reduced to a single C or N atom, respectively. H atoms are omitted. Colour Scheme: Mo teal, Co dark blue, P pink, O red, N blue, C black.

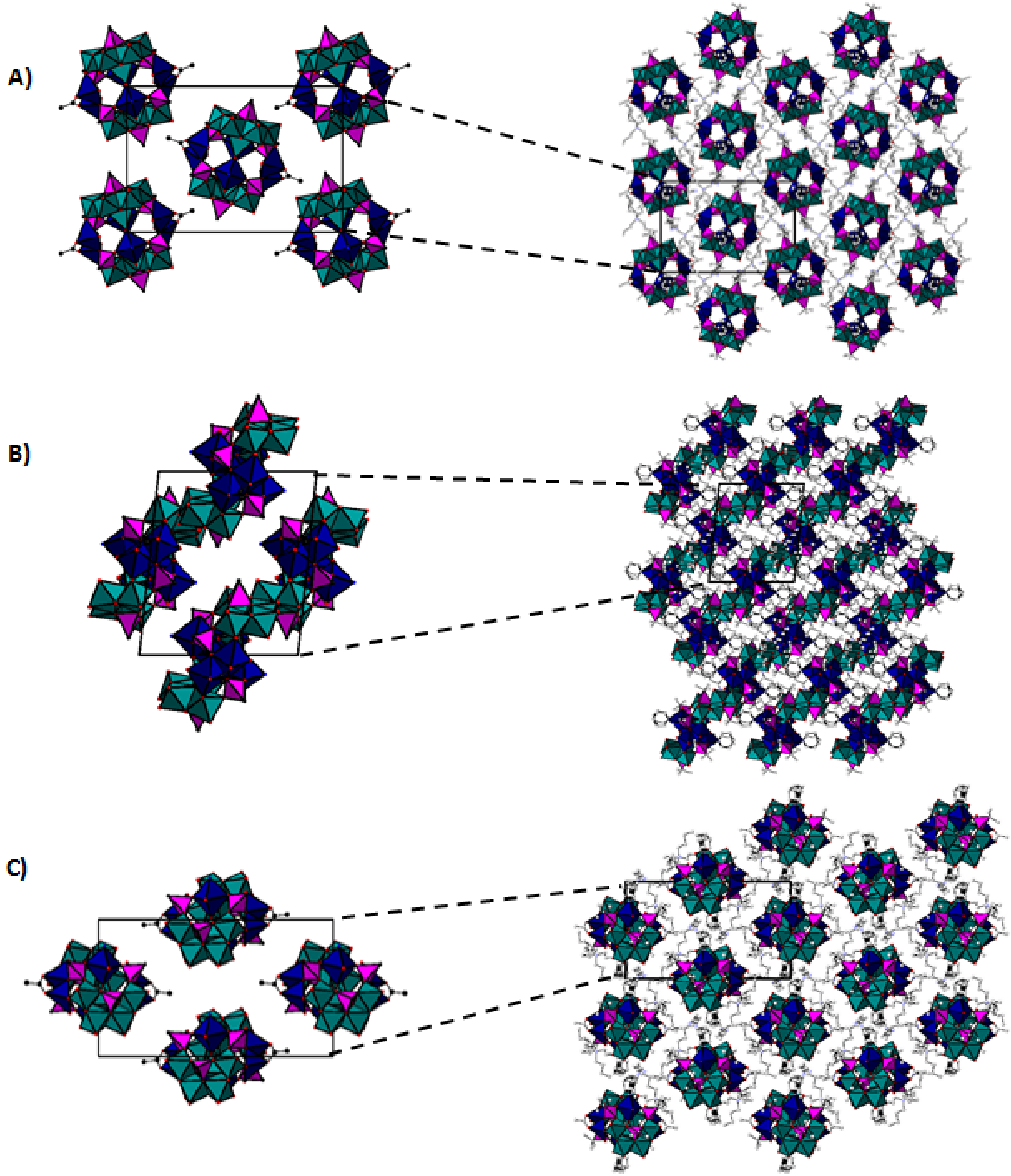

Figure S5. Packing diagrams for compound **1·3(MeCN),** as viewed along the crystallographic *a*-, *b*- and *c*-axes. Single unit cells (left) are shown in their reduced format (solvent and cations removed, *tert*-butyl and pyridyl groups reduced to single C or N atoms, H atoms omitted), for clarity. Full packing diagrams (right) are shown with C, H and N atoms partially faded, for clarity. Colour Scheme: Mo teal, Co dark blue, P pink, O red, N blue, C black, H white.

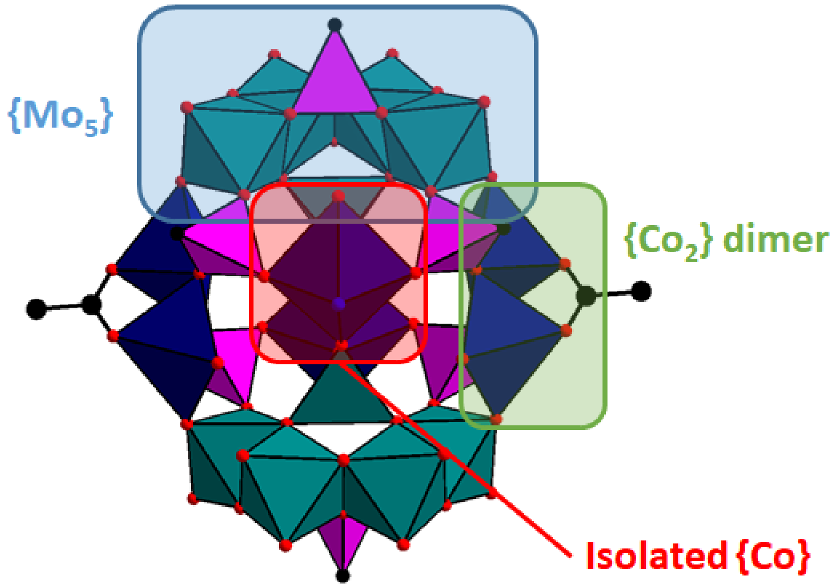

Figure S6. The anionic cluster in **1**, highlighting the {Mo_5}, {Co_2} and {Co} units. *Tert*-butyl and pyridyl groups are reduced to single C or N atoms. H atoms are omitted. Colour Scheme: Mo teal, Co dark blue, P pink, O red, N blue, C black, H white.

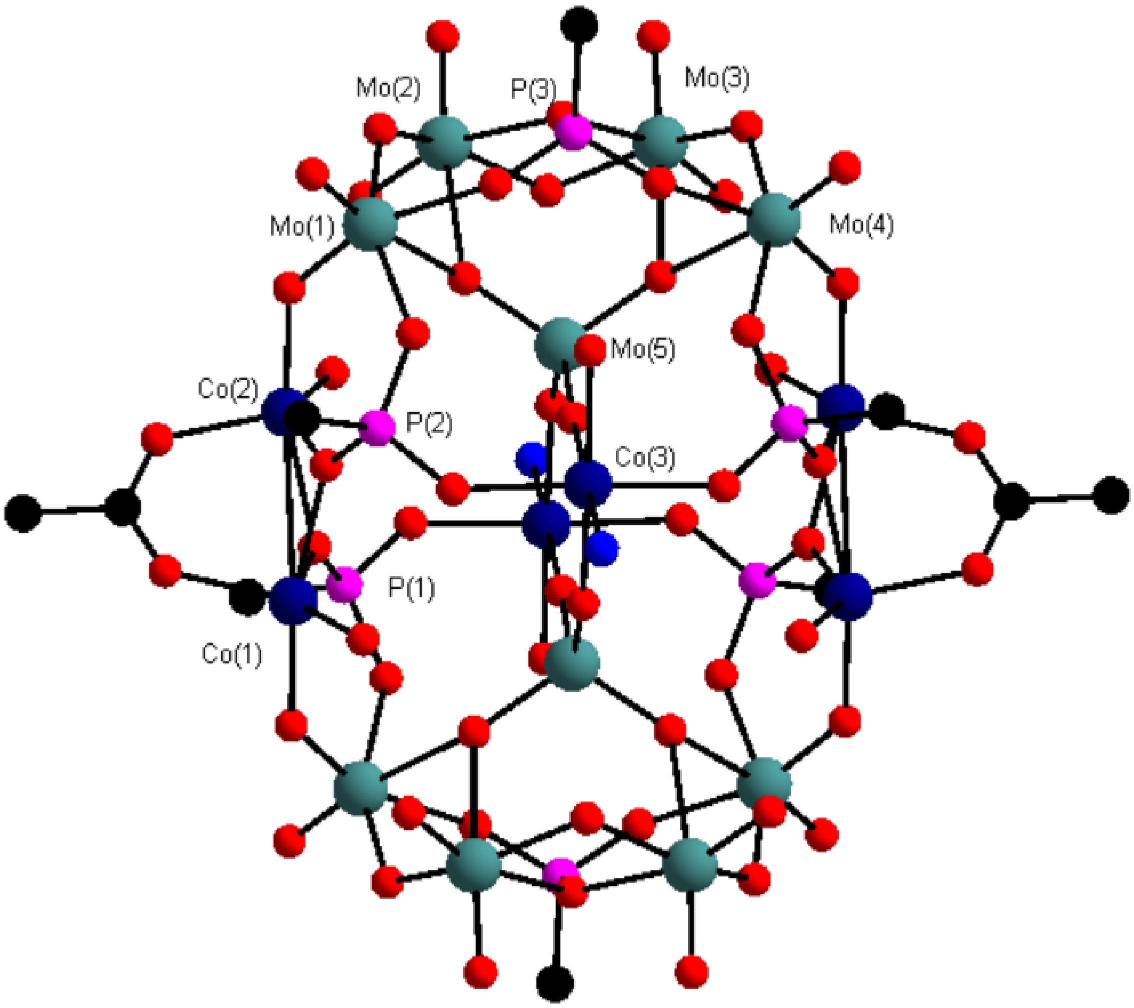

Figure S7. Atom numbering scheme for Mo, Co and P atoms in the anionic cluster in **1**. *Tert*-butyl and pyridyl groups are reduced to single C or N atoms. H atoms are omitted. Colour Scheme: Mo teal, Co dark blue, P pink, O red, N blue, C black.

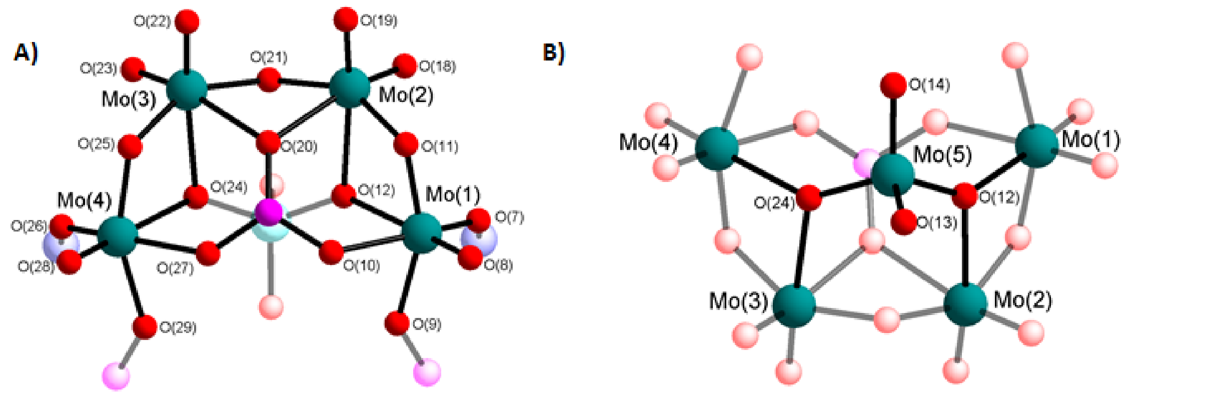

Figure S8. Atom numbering scheme for the {Mo_5} units in **1**. Colour Scheme: Mo teal, Co dark blue, P pink, O red. Atoms not directly bonded to Mo atoms are partially faded.

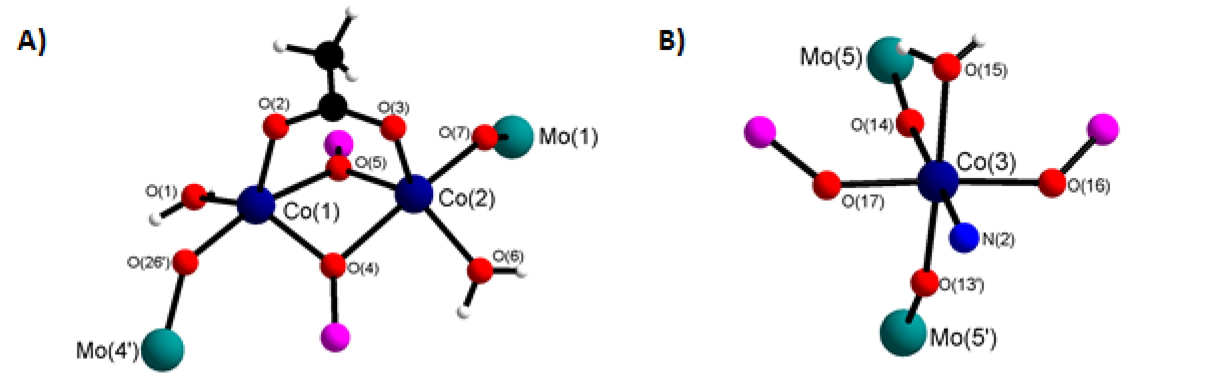

Figure S9. Atom numbering scheme for a) the {Co_2} and b) isolated {Co} units in **1**. Colour Scheme: Mo teal, Co dark blue, P pink, O red, N blue, C black, H white.

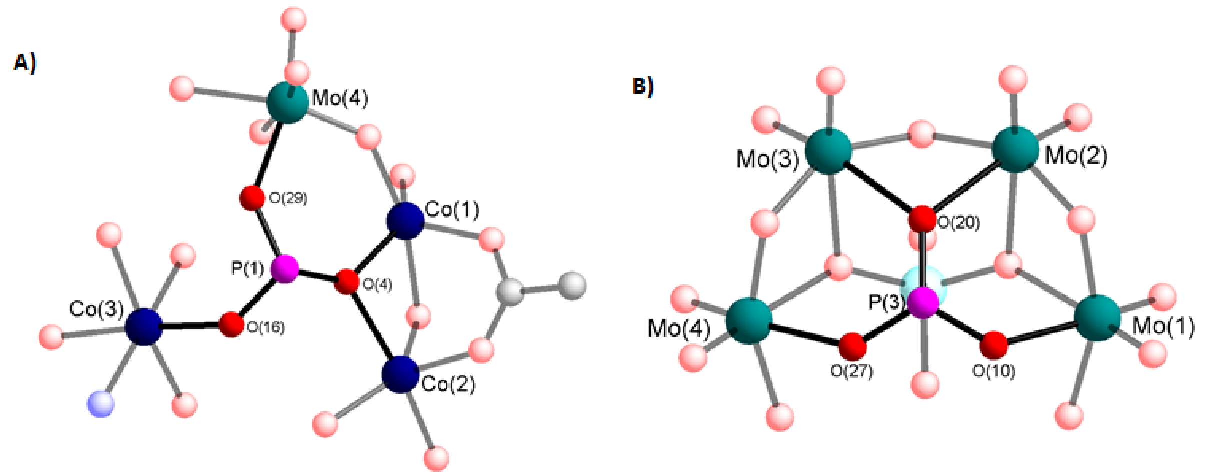

Figure S10. Atom numbering scheme for the two distinct phosphonate binding modes in **1**. P(2) coordinates in a similar fashion to P(1). Atoms not directly bonded to the phosphonate moieties are partially faded. *Tert*-butyl moieties are removed for clarity. Colour Scheme: Mo teal, Co dark blue, P pink, O red, N blue, C black.

3) Summary of Organic Ligands

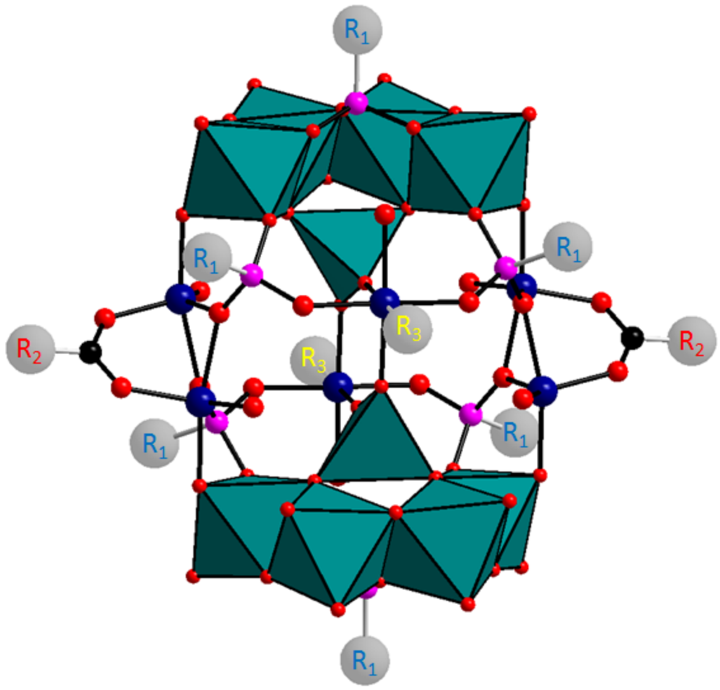

Figure S11. Diagram demonstrating the ligand binding sites in **1**, where R_1 represents a phosphonate moiety, R_2 represents a carboxylate moiety, and R_3 represents a pyridyl ligand.

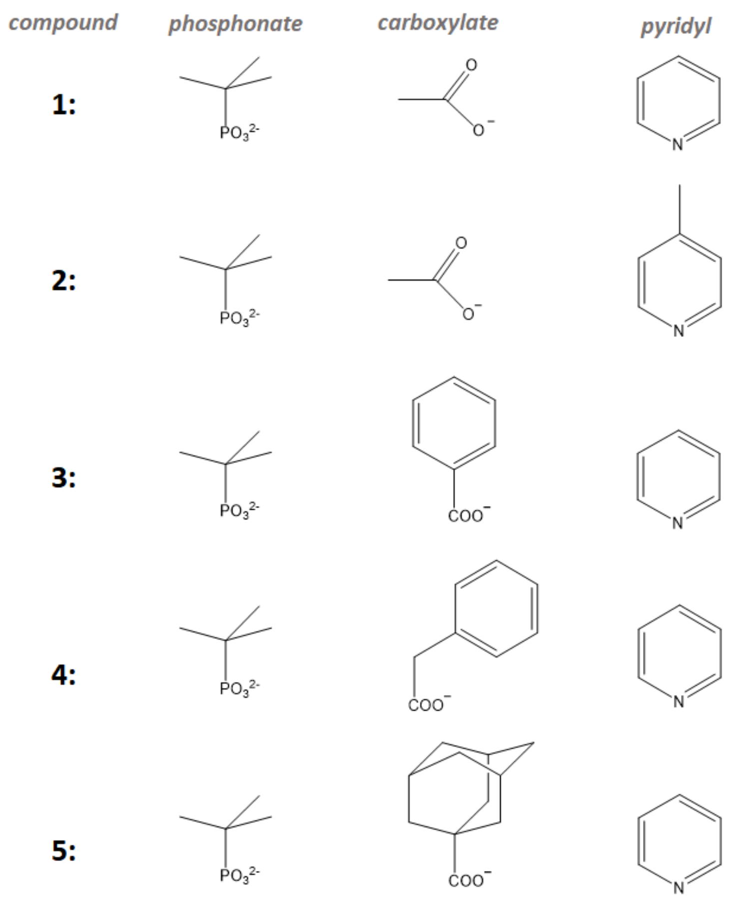

compound	*phosphonate*	*carboxylate*	*pyridyl*
6:	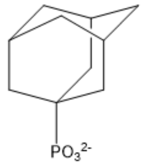	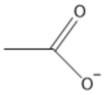	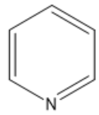
7:	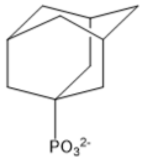	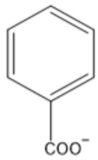	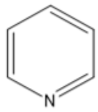
8:	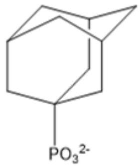	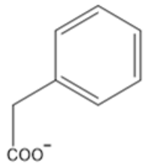	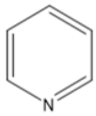
9:	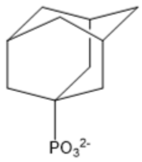	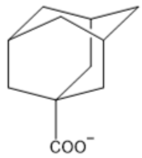	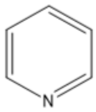
10:	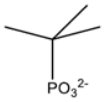	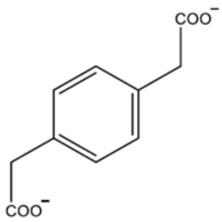	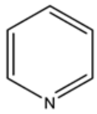

Table S1. Table summarising the phosphonate, carboxylate and pyridyl ligands in compounds **1** to **10**.

4) Additional pyridyl ligands in compound 2:

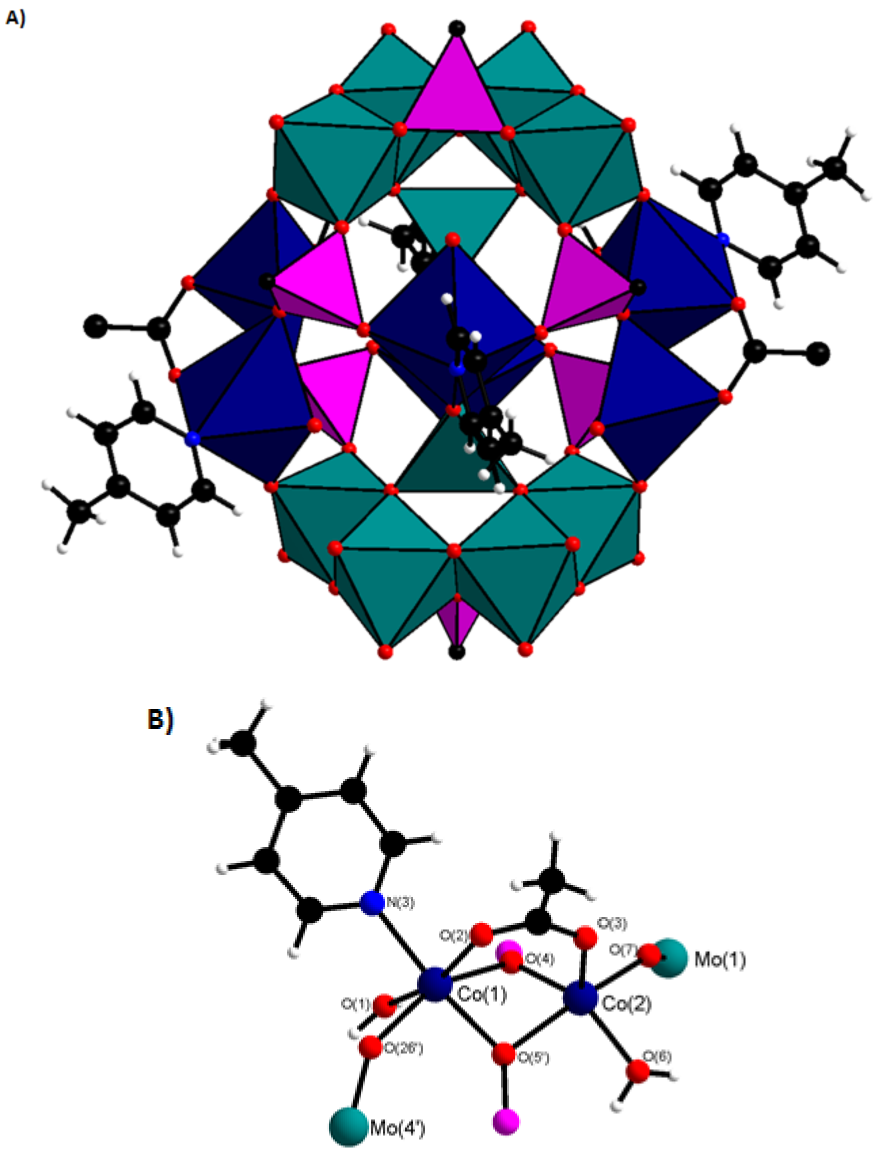

Figure S12. A) Structure of the anionic cluster in **2** in polyhedral representation, highlighting the additional pyridyl ligands which are incorporated into the structure. *Tert*-butyl groups are reduced to a single C atom. B) The coordination environment of the {Co_2} dimer, highlighting the incorporation of the picoline ligand. Colour Scheme: Mo teal, Co dark blue, P pink, O red, N blue, C black.

Additional pyridyl ligands are incorporated in this fashion in compounds **2**, **3** and **5**. Compound **8** contains two distinct cluster compounds in the crystal structure – one with four pyridyl ligands, and one with two.

5) Crystallographic Tables

Identification code	**1·3(MeCN)**
Empirical formula	$C_{76}H_{163}Co_6Mo_{10}N_7O_{58}P_6$
Formula weight (g/mol)	3601.92
Temperature (K)	100(2)
Wavelength (Å)	0.71073
Crystal system	Monoclinic
Space group	$P2_1/n$
a (Å)	14.9997(4)
b (Å)	25.6304(7)
c (Å)	17.4332(5)
α (°)	90
β (°)	96.0101(11)
γ (°)	90
Volume (Å^3)	6665.3(3)
Z	2
Calculated density ρ_{calc} (g/cm^3)	1.794
Absorption coefficient μ (mm^{-1})	1.786
F(000)	3608
Crystal size (mm^3)	0.190 x 0.180 x 0.160
2Θ range for data collection (°)	2.836 to 68.958
Index ranges	$-23 \le h \le 23$, $-40 \le k \le 40$, $-27 \le l \le 27$
Reflections collected	274655
Independent reflections	28146 [R_{int} = 0.0416]
Data/restraints/parameters	28146/49/779
Goodness-of-fit on F^2	1.006
Final R indices [I>=2σ (I)]	R_1 = 0.0302, wR_2 = 0.0731
Final R indices [all data]	R_1 = 0.0483, wR_2 = 0.0779
Largest diff. peak and hole (e Å^{-3})	2.034/-1.301

Table S2. Crystallographic details for compound **1.** One arm of the N(1) tetrabutlyammonium cation is crystallographically modelled as disordered over two positions with occupancy 50/50%. The pyridine ligand N(2) is crystallographically modelled as being disordered over three positions in a 30/40/30% ratio. Two solvent acetonitrile molecules, N(3) and N(4), are disordered over two positions each, with occupancy 50/50%.

Identification code	**2▪4.4(MeCN)**
Empirical formula	$C_{92.8}H_{185.2}Co_6Mo_{10}N_{10.4}O_{58}P_6$
Formula weight (g/mol)	3873.7
Temperature (K)	100(2)
Wavelength (Å)	0.71073
Crystal system	Triclinic
Space group	*P*-1
a (Å)	13.9147(6)
b (Å)	17.0418(7)
c (Å)	17.3781(7)
α (°)	74.8370(10)
β (°)	80.3310(10)
γ (°)	83.527(2)
Volume (Å^3)	3910.7(3)
Z	1
Calculated density ρ_{calc} (g/cm^3)	1.645
Absorption coefficient μ (mm^{-1})	1.529
F(000)	1951.0
Crystal size (mm^3)	0.11 x 0.1 x 0.09
2Θ range for data collection (°)	2.976 to 61.136
Index ranges	-19 ≤ h ≤ 19, -24 ≤ k ≤ 24, -24 ≤ l ≤ 24
Reflections collected	159269
Independent reflections	23891 [R_{int} = 0.0618]
Data/restraints/parameters	23891/41/923
Goodness-of-fit on F^2	1.093
Final R indices [I>=2σ (I)]	R_1 = 0.0460, wR_2 = 0.1089
Final R indices [all data]	R_1 = 0.0841, wR_2 = 0.1320
Largest diff. peak and hole (e Å^{-3})	1.79/-1.21

Table S3. Crystallographic details for compound **2.** Two arms of the tetrabutylammonium cations are modelled as being disordered in 0.43:0.57 and 0.32:0.68 ratios, respectively. One crystallographically distinct acetonitrile molecule is disordered over three positions in a 0.5:0.25:0.25 ratio, while another is 0.2 occupied.

Identification code	**3**
Empirical formula	$C_{90}H_{167}Co_6Mo_{10}N_6O_{58}P_6$
Formula weight (g/mol)	3910.7
Temperature (K)	100(2)
Wavelength (Å)	0.71073
Crystal system	Monoclinic
Space group	C2/c
a (Å)	21.7038(18)
b (Å)	24.446(2)
c (Å)	28.467(3)
α (°)	90.00
β (°)	109.836(1)
γ (°)	90.00
Volume ($Å^3$)	14208(2)
Z	4
Calculated density ρ_{calc} (g/cm^3)	1.758
Absorption coefficient μ (mm^{-1})	1.680
F(000)	7544.0
Crystal size (mm^3)	0.18 × 0.12 × 0.04
2Θ range for data collection (°)	3.042 to 56.608
Index ranges	$-28 \le h \le 28$, $-32 \le k \le 31$, $-37 \le l \le 23$
Reflections collected	55974
Independent reflections	17629 [R_{int} = 0.0464]
Data/restraints/parameters	17629/17/671
Goodness-of-fit on F^2	1.079
Final R indices [I>=2σ (I)]	R_1 = 0.0615, wR_2 = 0.1584
Final R indices [all data]	R_1 = 0.1086, wR_2 = 0.1956
Largest diff. peak and hole (e $Å^{-3}$)	1.93/-1.72

Table S4. Crystallographic details for compound **3.** No solvent molecules or solvent-accessible voids were observed crystallographically. The pyridine ligands on Co(3) are modelled as disordered over two positions in 0.51:0.49 ratios.

Identification code	**4·3.5(MeCN)**
Empirical formula	$C_{89}H_{172.5}Co_6Mo_{10}N_{7.5}O_{58}P_6$
Formula weight (g/mol)	3773.82
Temperature (K)	100(2)
Wavelength (Å)	0.71073
Crystal system	Monoclinic
Space group	$P2_1/n$
a (Å)	15.6966(7)
b (Å)	19.5580(9)
c (Å)	23.4785(10)
α (°)	90.00
β (°)	97.587
γ (°)	90.00
Volume (Å^3)	7144.7(6)
Z	2
Calculated density ρ_{calc} (g/cm^3)	1.754
Absorption coefficient μ (mm^{-1})	1.671
F(000)	3788.0
Crystal size (mm^3)	0.176 × 0.108 × 0.068
2Θ range for data collection (°)	2.95 to 59.338
Index ranges	$-21 \le h \le 28$, $-27 \le k \le 27$, $-32 \le l \le 32$
Reflections collected	246867
Independent reflections	20165 [R_{int} = 0.0738]
Data/restraints/parameters	20165/32/866
Goodness-of-fit on F^2	1.193
Final R indices [I>=2σ (I)]	R_1 = 0.0514, wR_2 = 0.1041
Final R indices [all data]	R_1 = 0.0836, wR_2 = 0.1185
Largest diff. peak and hole (e Å^{-3})	2.03/-1.36

Table S5. Crystallographic details for compound **4.** The terminal methyl groups on two arms of the tetrabutlyammonium cations are modelled as being disordered over two positions in 0.3:0.7 and 0.4:0.6 ratios, respectively. One crystallographically distinct acetonitrile molecule is disordered over two positions in a 0.56:0.44 ratio, and the other is 0.75 occupied.

Identification code	**5**
Empirical formula	$C_{98}H_{176}Co_6Mo_{10}N_6O_{58}P_6$
Formula weight (g/mol)	3865.24
Temperature (K)	100(2)
Wavelength (Å)	0.71073
Crystal system	Monoclinic
Space group	*C*2/c
a (Å)	22.2697(15)
b (Å)	24.3823(17)
c (Å)	28.6484(18)
α (°)	90.00
β (°)	110.0166(17)
γ (°)	90.00
Volume (Å^3)	14616.1(17)
Z	4
Calculated density ρ_{calc} (g/cm^3)	1.757
Absorption coefficient μ (mm^{-1})	1.635
F(000)	7768
Crystal size (mm^3)	0.280 × 0.070 × 0.060
2Θ range for data collection (°)	3.300 to 55.052
Index ranges	$-21 \le h \le 28$, $-31 \le k \le 31$, $-37 \le l \le 37$
Reflections collected	179819
Independent reflections	16792 [R_{int} = 0.0692]
Data/restraints/parameters	16792/79/858
Goodness-of-fit on F^2	1.086
Final R indices [I>=2σ (I)]	R_1 = 0.0563, wR_2 = 0.1383
Final R indices [all data]	R_1 = 0.0906, wR_2 = 0.1627
Largest diff. peak and hole (e Å^{-3})	1.494/-1.542

Table S6. Crystallographic details for compound **5.** The terminal methyl groups on two arms of the tetrabutlyammonium cations are modelled as being disordered over two positions in 0.44:0.56 and 0.41:0.59 ratios, respectively. One of the crystallographically distinct pyridine ligands is modelled as disordered over two positions in a 0.41:0.59 ratio. No solvent molecules or solvent-accessible voids were observed.

Identification code	**6•9.5(MeCN)**
Empirical formula	$C_{125}H_{218.5}Co_6Mo_{10}N_{13.5}O_{58}P_6$
Formula weight (g/mol)	4337.42
Temperature (K)	100(2)
Wavelength (Å)	0.71073
Crystal system	Monoclinic
Space group	$P2_1/n$
a (Å)	17.6667(8)
b (Å)	25.3666(12)
c (Å)	20.0291(9)
α (°)	90
β (°)	107.6720(10)
γ (°)	90
Volume (Å^3)	8552.3(7)
Z	2
Calculated density ρ_{calc} (g/cm^3)	1.684
Absorption coefficient μ (mm^{-1})	1.409
F(000)	4398.0
Crystal size (mm^3)	0.15 × 0.12 × 0.05
2Θ range for data collection (°)	2.67 to 52.234
Index ranges	$-21 \le h \le 21$, $-31 \le k \le 31$, $-24 \le l \le 24$
Reflections collected	104339
Independent reflections	16945 [R_{int} = 0.0909]
Data/restraints/parameters	16945/83/1006
Goodness-of-fit on F^2	0.889
Final R indices [I>=2σ (I)]	R_1 = 0.0356, wR_2 = 0.0643
Final R indices [all data]	R_1 = 0.0817, wR_2 = 0.0730
Largest diff. peak and hole (e Å^{-3})	1.04/-1.22

Table S7. Crystallographic details for compound **6.** Of the five crystallographically distinct acetonitrile molecules, two are fully occupied, one is modelled as disordered in a 0.72/0.28 ratio, one in a 0.75/0.25 ratio, and the fifth is modelled as being 0.75 occupied, split over two positions in a 0.25/0.5 ratio.

Identification code	**7·2(MeCN)**
Empirical formula	$C_{240}H_{354}Co_{12}Mo_{20}N_{12}O_{116}P_{12}$
Formula weight (g/mol)	8260.93
Temperature (K)	100(2)
Wavelength (Å)	0.71073
Crystal system	Monoclinic
Space group	*C*2/m
a (Å)	29.7884(13)
b (Å)	28.1953(12)
c (Å)	19.9483(8)
α (°)	90
β (°)	91.4630(10)
γ (°)	90
Volume (Å^3)	16749.0(12)
Z	2
Calculated density ρ_{calc} (g/cm^3)	1.638
Absorption coefficient μ (mm^{-1})	1.433
F(000)	8300.0
Crystal size (mm^3)	0.14 × 0.13 × 0.06
2Θ range for data collection (°)	2.736 to 51.566
Index ranges	$-36 \le h \le 36$, $-34 \le k \le 34$, $-24 \le l \le 22$
Reflections collected	157139
Independent reflections	16357 [R_{int} = 0.0738]
Data/restraints/parameters	16357/145/938
Goodness-of-fit on F^2	1.068
Final R indices [I>=2σ (I)]	R_1 = 0.0698, wR_2 = 0.1668
Final R indices [all data]	R_1 = 0.1279, wR_2 = 0.2192
Largest diff. peak and hole (e Å^{-3})	2.77/-2.14

Table S8. Crystallographic details for compound **7.** The pyridine ligands are modelled as disordered over two positions in a 50/50 ratio. The terminal carbon one arm of the tetrabutylammonium cation is modelled as disordered over two positions in a 0.61/0.39 ratio. Constraints (DFIX and DANG) were used on the adamantyl groups.

Identification code	**8·5(MeCN)**
Empirical formula	$C_{133}H_{203}Co_6Mo_{10}N_{10}O_{58}P_6$
Formula weight (g/mol)	4368.84
Temperature (K)	100(2)
Wavelength (Å)	0.71073
Crystal system	Triclinic
Space group	*P*-1
a (Å)	17.7506(7)
b (Å)	18.8983(8)
c (Å)	27.1892(12)
α (°)	75.8350(10)
β (°)	80.8820(10)
γ (°)	72.5210(10)
Volume (Å^3)	8399.5(6)
Z	2
Calculated density ρ_{calc} (g/cm^3)	1.727
Absorption coefficient μ (mm^{-1})	1.435
F(000)	4414.0
Crystal size (mm^3)	0.14 × 0.1 × 0.07
2Θ range for data collection (°)	2.748 to 52.994
Index ranges	$-22 \le h \le 22$, $-23 \le k \le 23$, $-34 \le l \le 34$
Reflections collected	202902
Independent reflections	34616 [R_{int} = 0.0895]
Data/restraints/parameters	34616/1/1956
Goodness-of-fit on F^2	1.009
Final R indices [I>=2σ (I)]	R_1 = 0.0439, wR_2 = 0.0957
Final R indices [all data]	R_1 = 0.0883, wR_2 = 0.1160
Largest diff. peak and hole (e Å^{-3})	1.94/-1.83

Table S9. Crystallographic details for compound **8.**

Identification code	**9·6(MeCN)**
Empirical formula	$C_{136}H_{130}Co_6Mo_{10}N_{10}O_{58}P_6$
Formula weight (g/mol)	4331.29
Temperature (K)	100(2)
Wavelength (Å)	0.71073
Crystal system	Triclinic
Space group	*P*-1
a (Å)	16.9115(8)
b (Å)	17.8098(9)
c (Å)	18.2776(9)
α (°)	65.2690(10)
β (°)	64.0720(10)
γ (°)	84.8630(10)
Volume (Å^3)	4467.4(4)
Z	1
Calculated density ρ_{calc} (g/cm^3)	1.610
Absorption coefficient μ (mm^{-1})	1.349
F(000)	2152.0
2Θ range for data collection (°)	2.696 to 59.09
Index ranges	$-23 \leq h \leq 23$, $-24 \leq k \leq 24$, $-25 \leq l \leq 25$
Reflections collected	152064
Independent reflections	24963 [R_{int} = 0.0528]
Data/restraints/parameters	24963/4/971
Goodness-of-fit on F^2	1.022
Final R indices [I>=2σ (I)]	R_1 = 0.0622, wR_2 = 0.1622
Final R indices [all data]	R_1 = 0.0986, wR_2 = 0.1969
Largest diff. peak and hole (e Å^{-3})	2.95/-1.75

Table S10. Crystallographic details for compound **9.** The adamantyl groups on the carboxylate ligands are modelled as being rotationally disordered over two positions in a 0.59/0.41 ratio. The tetrabutylammonium cation is highly disordered. H atom positions were not calculated for the tetrabutylammonium cation or for the solvent molecules. Of the three crystallographically distinct acetonitrile molecules, two are modelled as fully occupied and the third is modelled as disordered over two positions with 50/50 occupancy.

Identification code	**10·7.5(MeCN)**
Empirical formula	$C_{45.5}H_{87.25}Co_3Mo_5N_{5.75}O_{29}P_3$
Formula weight (g/mol)	1928.36
Temperature (K)	100(2)
Wavelength (Å)	0.71073
Crystal system	Triclinic
Space group	*P*-1
a (Å)	13.7500(4)
b (Å)	16.8554(5)
c (Å)	17.1095(5)
α (°)	107.6320(10)
β (°)	95.0120(10)
γ (°)	101.6640(10)
Volume (Å^3)	3653.79(19)
Z	2
Calculated density ρ_{calc} (g/cm^3)	1.753
Absorption coefficient μ (mm^{-1})	1.636
F(000)	1937.0
Crystal size (mm^3)	0.131 × 0.076 × 0.04
2Θ range for data collection (°)	3.064 to 62.178
Index ranges	$-19 \le h \le 19$, $-24 \le k \le 22$, $-23 \le l \le 24$
Reflections collected	73920
Independent reflections	22705 [R_{int} = 0.0889]
Data/restraints/parameters	22705/8/848
Goodness-of-fit on F^2	1.002
Final R indices [I>=2σ (I)]	R_1 = 0.0544, wR_2 = 0.0903
Final R indices [all data]	R_1 = 0.1150, wR_2 = 0.1056
Largest diff. peak and hole (e Å^{-3})	1.64/-1.01

Table S11. Crystallographic details for compound **10.** Of the four crystallographically distinct acetonitrile solvent molecules, three are modelled as fully occupied and one is modelled with 0.75 occupancy.

6) Bond Lengths and Angles for Compound 1

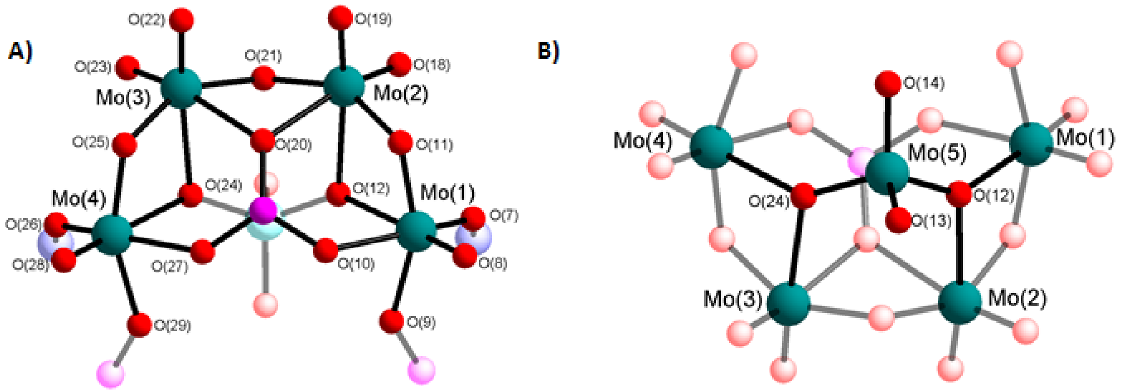

Figure S13. Atom labelling scheme for the molybdate moieties in **1**.

Metal Atom	Bonded Atom	Bond Length (Å)	BVS	Oxidation State
Mo(1)	O(8)	1.688(2)	6.086	+VI
	O(7)	1.753(1)		
	O(11)	1.873(2)		
	O(9)	2.027(1)		
	O(10)	2.084(1)		
	O(12)	2.328(1)		
Mo(2)	O(19)	1.695(2)	5.985	+VI
	O(18)	1.717(2)		
	O(21)	1.920(1)		
	O(11)	1.923(1)		
	O(20)	2.308(1)		
	O(12)	2.382(1)		
Mo(3)	O(22)	1.694(2)	5.968	+VI
	O(23)	1.719(2)		
	O(21)	1.916(1)		
	O(25)	1.932(1)		
	O(20)	2.328(1)		
	O(24)	2.357(1)		
Mo(4)	O(28)	1.690(1)	6.063	+VI
	O(26)	1.748(1)		
	O(25)	1.878(1)		
	O(29)	2.034(2)		
	O(27)	2.085(1)		
	O(24)	2.328(1)		
Mo(5)	O(14)	1.721(1)	5.858	+VI
	O(13)	1.741(1)		
	O(12)	1.804(1)		
	O(24)	1.805(1)		

Table S12. Bond lengths for the molybdate moieties in **1**, along with bond valence sum (BVS) values and the assigned oxidation state for each molybdenum atom.

Short bond lengths (*c.* 1.7 Å) represent either terminal Mo=O bonds or bridging Mo-O-Co bonds. Bonds of *c.* 1.9 Å represent Mo-O-Mo briding modes. Mo-OP bond lengths vary widely, in the range of 2.0 Å to 2.35 Å. The μ_3-O ligands O(12) and O(24) display short bond lengths to the tetrahedral Mo centre (roughly 1.8 Å) and longer bonds to the other Mo centres (Mo(1)-Mo(4), roughly 2.35 Å).

BVS represents the Bond Valence Sum parameter, which was used to assign oxidation states.

Bond	Bond Angle (°)	Bond	Bond Angle (°)
O(11)-Mo(1)-O(12)	75.87(5)	O(21)-Mo(2)-O(20)	73.29(5)
O(10)-Mo(1)-O(12)	76.94(5)	O(11)-Mo(2)-O(12)	73.68(5)
O(9)-Mo(1)-O(10)	78.19(5)	O(20)-Mo(2)-O(12)	74.96(5)
O(9)-Mo(1)-O(12)	82.46(5)	O(21)-Mo(2)-O(12)	79.24(5)
O(7)-Mo(1)-O(12)	84.02(6)	O(11)-Mo(2)-O(20)	81.27(6)
O(11)-Mo(1)-O(10)	84.85(6)	O(18)-Mo(2)-O(12)	87.85(6)
O(7)-Mo(1)-O(9)	90.21(6)	O(19)-Mo(2)-O(20)	92.78(6)
O(8)-Mo(1)-O(10)	96.21(7)	O(18)-Mo(2)-O(21)	98.10(7)
O(7)-Mo(1)-O(11)	99.64(6)	O(18)-Mo(2)-O(11)	99.75(7)
O(8)-Mo(1)-O(9)	99.88(7)	O(19)-Mo(2)-O(11)	100.09(7)
O(8)-Mo(1)-O(11)	100.09(7)	O(19)-Mo(2)-O(21)	102.13(7)
O(8)-Mo(1)-O(7)	103.31(7)	O(19)-Mo(2)-O(18)	104.79(7)
Angle Variance (σ^2)	**103.4**	**Angle Variance (σ^2)**	**145.9**
Distortion Index	**0.100**	**Distortion Index**	**0.119**
O(21)-Mo(3)-O(20)	72.86(5)	O(25)-Mo(4)-O(24)	75.69(5)
O(25)-Mo(3)-O(24)	74.05(5)	O(27)-Mo(4)-O(24)	76.94(5)
O(20)-Mo(3)-O(24)	75.24(4)	O(29)-Mo(4)-O(27)	78.09(5)
O(21)-Mo(3)-O(24)	79.96(5)	O(29)-Mo(4)-O(24)	83.36(5)
O(25)-Mo(3)-O(20)	81.27(5)	O(26)-Mo(4)-O(24)	84.43(5)
O(23)-Mo(3)-O(24)	87.93(6)	O(25)-Mo(4)-O(27)	85.64(6)
O(22)-Mo(3)-O(20)	92.40(6)	O(26)-Mo(4)-O(29)	89.75(6)
O(22)-Mo(3)-O(25)	98.83(7)	O(28)-Mo(4)-O(27)	95.68(7)
O(23)-Mo(3)-O(21)	98.86(7)	O(28)-Mo(4)-O(29)	99.52(6)
O(23)-Mo(3)-O(25)	99.89(7)	O(28)-Mo(4)-O(25)	99.65(7)
O(22)-Mo(3)-O(21)	102.08(7)	O(26)-Mo(4)-O(25)	99.74(6)
O(22)-Mo(3)-O(23)	104.88(7)	O(28)-Mo(4)-O(26)	103.57(7)
Angle Variance (σ^2)	**143.2**	**Angle Variance (σ^2)**	**100.6**
Distortion Index	**0.118**	**Distortion Index**	**0.096**
O(14)-Mo(2)-O(24)	108.66(6)		
O(14)-Mo(2)-O(12)	109.09(6)		
O(13)-Mo(2)-O(12)	109.19(6)		
O(14)-Mo(2)-O(13)	109.47(6)		
O(13)-Mo(2)-O(24)	109.56(6)		
O(12)-Mo(2)-O(24)	110.85(6)		
Geometry Index (τ_4)	**0.990**		

Table S13. Bond angles for the molybdate moieties in **1**, along with distortion parameters for each Mo center.

The Bond Angle Variance (σ^2_{oct}) and the Distortion Index (DI) are two methods to quantify the extent of distortion away from idealised octahedral geometry. The Bond Angle Variance is defined as:

$$\sigma^2_{oct} = \frac{1}{11}\sum_{i=1}^{12}(\alpha_i - 90°)^2$$

α represents a bond angle in the system (only the angles between *cis*- bonded ligands are considered). σ^2_{oct} = 0 represents a perfect octahedron.[3]

The Distortion Index is defined as:

$$DI = \frac{1}{12\alpha_m}\sum_{i=1}^{12}|\alpha_i - \alpha_m|$$

α_i and α_m represent an individual bond angle and the average bond angle, respectively (again, considering only *cis*- bonded ligands).[4,5] Again DI = 0 reflects an ideal, undistorted octahedron.

The σ^2_{oct} values range from 100.6 to 145.9, indicating that the coordination octahedra in the system are highly distorted, particularly for Mo(2) and Mo(3) (Table S13). DI values also demonstrate distortion, ranging from 0.096 to 0.119. The significant distortion in the octahedral coordination environments reflects the variety of O-donor ligands (terminal *O*- ligands, bridging μ-O and triply bridging μ_3-O ligands, monodentate phosphonates and bridging phosphonates).

In contrast, the tetrahedral coordination environment of Mo(5) is extremely close to an ideal tetrahedron (τ_4 = 0.990, where τ_4 = 1 represents an ideal tetrahedron). The four coordinate geometry index τ_4 is defined as:

$$\tau_4 = \frac{360° - (\alpha_1 + \alpha_2)}{360° - 2\theta}$$

α_1 and α_2 represent the largest and second largest bond angles in the system, respectively. θ represents the ideal tetrahedral angle (*c.* 109.5°).[6]

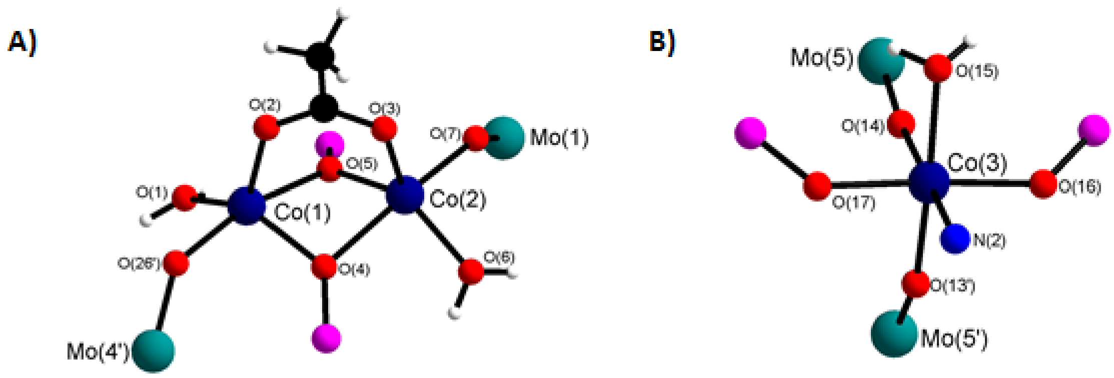

Figure S14. Atom labelling scheme for the cobalt moieties in **1**.

Metal Atom	Bonded Atom	Bond Length (Å)	BVS	Oxidation State
Co(1)	O(1)	1.975(1)	2.015	+II
	O(2)	1.982(2)		
	O(4)	1.988(1)		
	O(26’)	2.047(1)		
	O(5)	2.189(2)		
Co(2)	O(6)	1.981(1)	2.005	+II
	O(3)	1.985(2)		
	O(5)	1.991(1)		
	O(7)	2.044(1)		
	O(4)	2.187(2)		
Co(3)	O(16)	2.051(1)	1.971	+II
	O(17)	2.054(1)		
	O(13’)	2.069(1)		
	N(2)	2.140(3)		
	O(15)	2.143(1)		
	O(14)	2.190(1)		

Table S14. Bond lengths for the cobalt moieties in **1**, along with bond valence sum (BVS) values and the assigned oxidation state for each cobalt atom.

In the dinuclear unit (Co(1) and Co(2)), water, acetate and bridging *oxo* ligands all display bond lengths of *c.* 2.0 Å. However the phosphonate O-donors O(4) and O(5) are skewed – O(4) is about 0.2 Å closer to Co(1) than Co(2), and *vice versa* for O(5).

BVS represents the bond valence sum parameter and was used to assign oxidation states.

Bond	Bond Angle (°)	Bond	Bond Angle (°)
O(4)-Co(1)-O(5)	81.05(5)	O(5)-Co(2)-O(4)	81.03(5)
O(1)-Co(1)-O(5)	85.57(5)	O(6)-Co(2)-O(4)	85.52(5)
O(2)-Co(1)-O(5)	89.98(6)	O(5)-Co(2)-O(7)	90.61(5)
O(4)-Co(1)-O(26’)	90.60(6)	O(3)-Co(2)-O(4)	91.21(6)
O(1)-Co(1)-O(26’)	93.46(6)	O(6)-Co(2)-O(7)	94.30(6)
O(2)-Co(1)-O(4)	95.85(6)	O(3)-Co(2)-O(5)	99.95(6)
O(2)-Co(1)-O(26’)	102.02(6)	O(3)-Co(2)-O(7)	101.11(6)
O(1)-Co(1)-O(2)	123.65(7)	O(3)-Co(2)-O(6)	116.96(6)
O(1)-Co(1)-O(4)	138.23(6)	O(5)-Co(2)-O(6)	140.90(6)
O(5)-Co(1)-O(26’)	166.08(6)	O(4)-Co(2)-O(7)	166.18(6)
Geometry Index (τ_5)	**0.464**	**Geometry Index (τ_5)**	**0.421**
O(15)-Co(3)-O(14)	83.06(5)		
O(17)-Co(3)-N(2)	84.9(2)		
O(13’)-Co(3)-O(14)	87.27(5)		
O(16)-Co(3)-N(2)	87.8(2)		
O(13’)-Co(3)-N(2)	88.37(18)		
O(16)-Co(3)-O(15)	90.08(5)		
O(17)-Co(3)-O(15)	90.22(5)		
O(17)-Co(3)-O(13’)	90.23(5)		
O(16)-Co(3)-O(13’)	90.72(5)		
O(17)-Co(3)-O(14)	92.60(5)		
O(16)-Co(3)-O(14)	94.80(5)		
N(2)-Co(3)-O(15)	101.29(18)		
Angle Variance (σ^2)	**22.5**		
Distortion Index	**0.035**		

Table S15. Bond angles for the cobalt moieties in **1**, along with distortion parameters for each Co center.

The five-coordinate geometry index (τ_5) provides a metric to quantify the distortion from the idealised square planar geometry. The geometry index is defined as:

$$\tau_5 = \frac{\alpha_1 - \alpha_2}{60°}$$

α_1 and α_2 represent the largest and second largest bond angles in the system, respectively. [7] For an ideal square pyramid τ_5 = 0 and for an ideal trigonal bipyramid τ_5 = 1.

Co(1) and Co(2) both display highly distorted square pyramidal coordination geometries. This high level of distortion may explain why some analogues of **1** incorporate additional pyridyl ligands onto the dinuclear units, allowing one Co ion in the dinuclear unit to adopt an octahedral geometry

The octahedral centre Co(3) shows very low levels of distortion, with σ^2_{oct} and DI values close to the ideal of zero.

7) Intramolecular Hydrogen Bonding Network

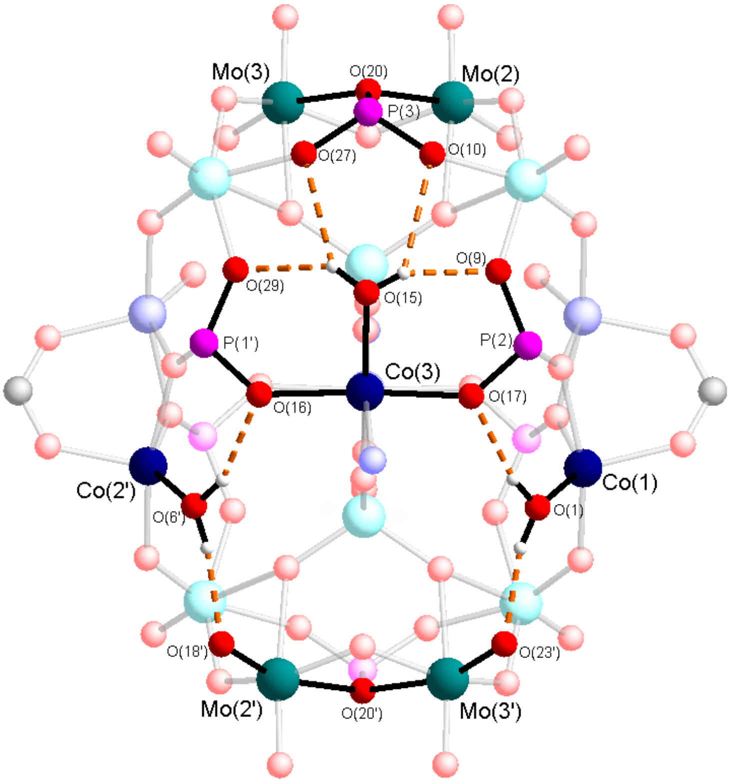

Figure S15. The anionic cluster in **1**, highlighting the intramolecular hydrogen-bonding network. Each face of the cluster core in 5 engages in a network of hydrogen-bonding interactions between the H-donor water molecules in the cluster (O(1), O(6), and O(15)) and a series of H-acceptor terminal *oxo-* ligands (O(18) and O(23)) and phosphonate oxygens (O(9), O(10), O(27), O(29), O(16) and O(17)).

Atom	Bond Valence Sum	Assignment
O(1)	0.465	H_2O
O(6)	0.460	H_2O
O(15)	0.300	H_2O

Table S16. Bond Valence Sum (BVS) for the O-donor ligands O(1), O(6) and O(15) confirms the identities of these ligands as monodentate water ligands. BVS values for an oxygen atom in the approximate range 1.8-2.0 indicates *oxo-* ligands, 1.0-1.2 indicates hydroxo ligands, and values in the 0.2-0.4 range indicate water ligands. Hydrogen atoms could not be located crystallographically and so their positions are calculated.

8) MALDI Mass Spectrometry of Compound 1

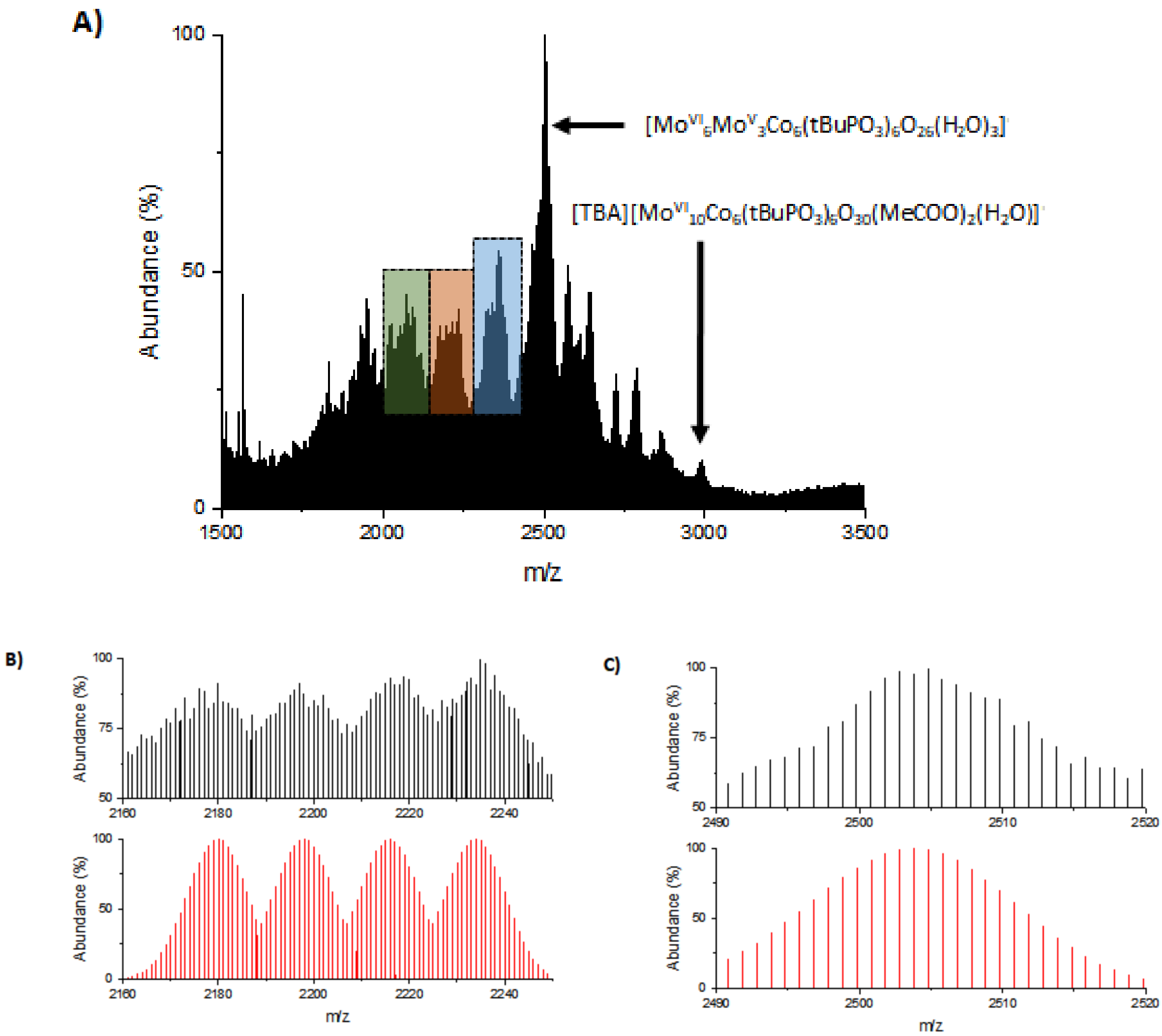

Figure S16. A) The negative-mode MALDI-MS of compound **1** in acetonitrile. B) Experimental (black) and simulated (red) spectra for the orange-shaded region in A. C) Experimental (black) and simulated (red) spectra for the $[Mo^{VI}_6Mo^{V}_3Co_6(tBuPO_3)_6O_{26}(H_2O)_3]^-$ peak.

The largest observable species in the MALDI-MS spectrum of compound **1** in acetonitrile can be assigned as $[TBA][Mo_{10}Co_6(tBuPO_3)_6O_{30}(MeCOO)_2(H_2O)]^-$ (expected mass 2900.00, observed mass 2900.01), which corresponds to the loss of two pyridine and five water molecules from **1**. Interestingly, several decomposition products can be observed in the spectrum as the compound loses the peripheral ligands followed by a series of successive $\{MoO_x\}$ fragments. The most intense peak observed in the spectrum is $[Mo^{VI}_6Mo^{V}_3Co_6(tBuPO_3)_6O_{26}(H_2O)_3]^-$, followed by a series of smaller fragments. These fragments come in clusters of four peaks, representing different protonation/charge states.

Species	*m/z calc.*	*m/z obs.*
$[TBA][Mo_{10}Co_6(tBuPO_3)_6O_{30}(MeCOO)_2(H_2O)]^-$	*2900.00*	*2900.01*
$[Mo^{VI}{}_6Mo^{V}{}_3Co_6(tBuPO_3)_6O_{26}(H_2O)_3]^-$	*2503.83*	*2503.79*
$[Mo^{VI}{}_8Mo^{V}Co_6(tBuPO_3)_6O_{27}]^-$	*2465.79*	*2465.80*
$[Mo^{VI}{}_5Mo^{V}{}_3Co_6(tBuPO_3)_6O_{23}(H_2O)_4]^-$	*2377.94*	*2377.87*
$[Mo^{VI}{}_5Mo^{V}{}_3Co_6(tBuPO_3)_6O_{23}(H_2O)_3]^-$	*2359.93*	*2359.89*
$[Mo^{VI}{}_5Mo^{V}{}_3Co_6(tBuPO_3)_6O_{23}(H_2O)_2]^-$	*2341.93*	*2341.88*
$[Mo^{VI}{}_5Mo^{V}{}_3Co_6(tBuPO_3)_6O_{23}(H_2O)]^-$	*2323.91*	*2323.89*
$[Mo^{VI}{}_3Mo^{V}{}_4Co_6(tBuPO_3)_6O_{20}(H_2O)_4]^-$	*2235.05*	*2234.97*
$[Mo^{VI}{}_3Mo^{V}{}_4Co_6(tBuPO_3)_6O_{20}(H_2O)_3]^-$	*2216.04*	*2216.00*
$[Mo^{VI}{}_3Mo^{V}{}_4Co_6(tBuPO_3)_6O_{20}(H_2O)_2]^-$	*2197.03*	*2196.96*
$[Mo^{VI}{}_3Mo^{V}{}_4Co_6(tBuPO_3)_6O_{20}(H_2O)_1]^-$	*2180.02*	*2179.98*
$[Mo^{IV}Mo^{V}{}_5Co_6(tBuPO_3)_6O_{15}(H_2O)_6]^-$	*2095.20*	*2095.02*
$[Mo^{IV}Mo^{V}{}_5Co_6(tBuPO_3)_6O_{15}(H_2O)_5]^-$	*2076.18*	*2076.02*
$[Mo^{IV}Mo^{V}{}_5Co_6(tBuPO_3)_6O_{15}(H_2O)_4]^-$	*2057.17*	*2057.01*
$[Mo^{IV}Mo^{V}{}_5Co_6(tBuPO_3)_6O_{15}(H_2O)_2]^-$	*2023.15*	*2023.03*

Table S17. Observed peaks in the negative-mode MALDI-MS spectrum of compound **1** in acetonitrile.

9) Comparison of Molybdate Fragment with Octamolybdate and Strangberg Compounds

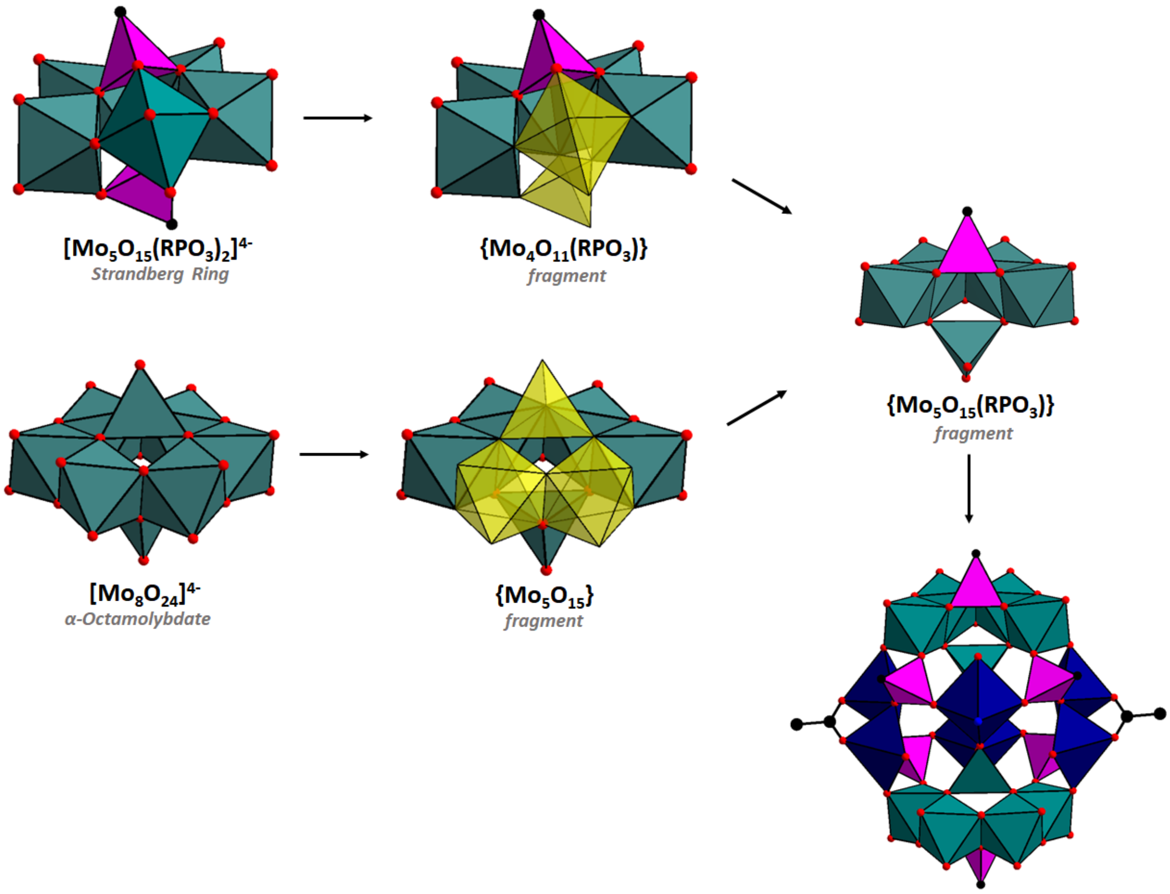

Figure S17. Diagram showing the relationship between the previously-reported Strandberg and α-octamolybdate compounds, and the molybdate fragment in compounds **1** to **10**.

10) TGA Analysis For Compounds 1-10

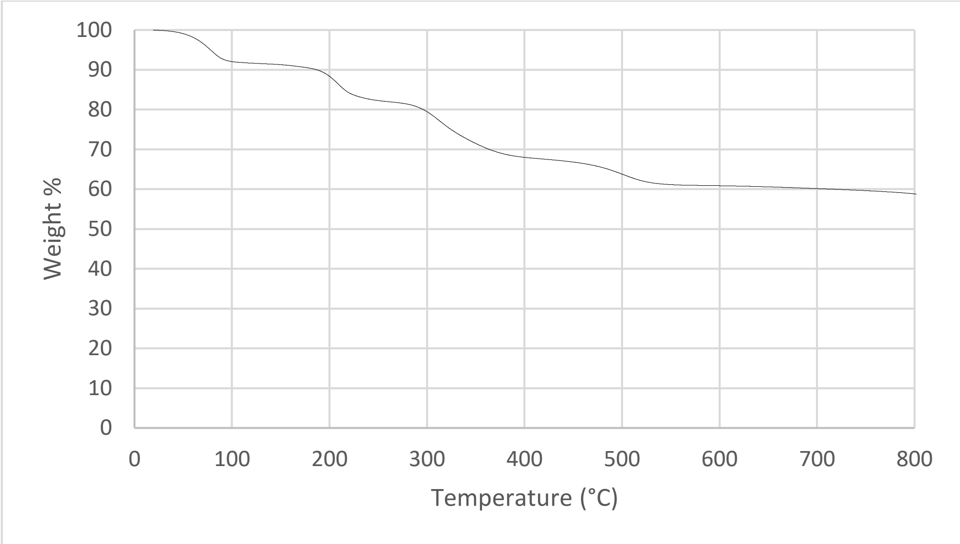

Figure S18. TGA analysis for compound **1** (recorded in N_2 atmosphere; heating rate 10 ^oC/min.)

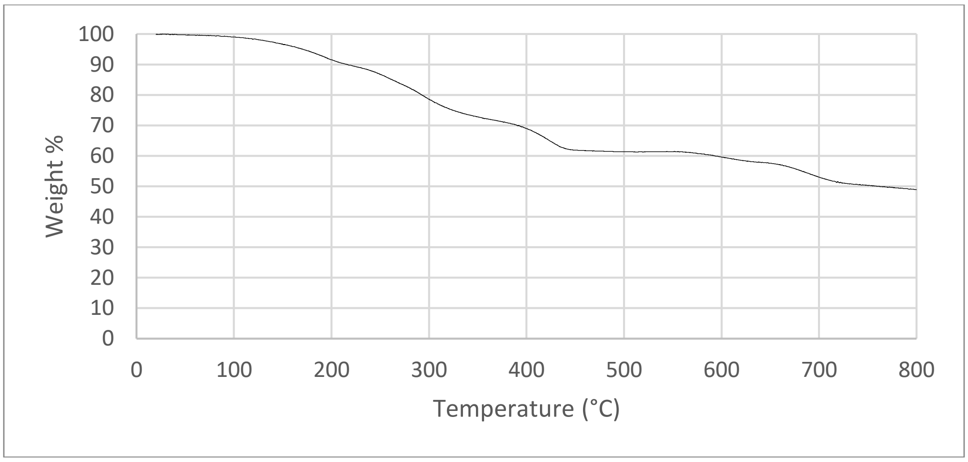

Figure S19. TGA analysis for compound **2**(recorded in N_2 atmosphere; heating rate 10 ^oC/min.)

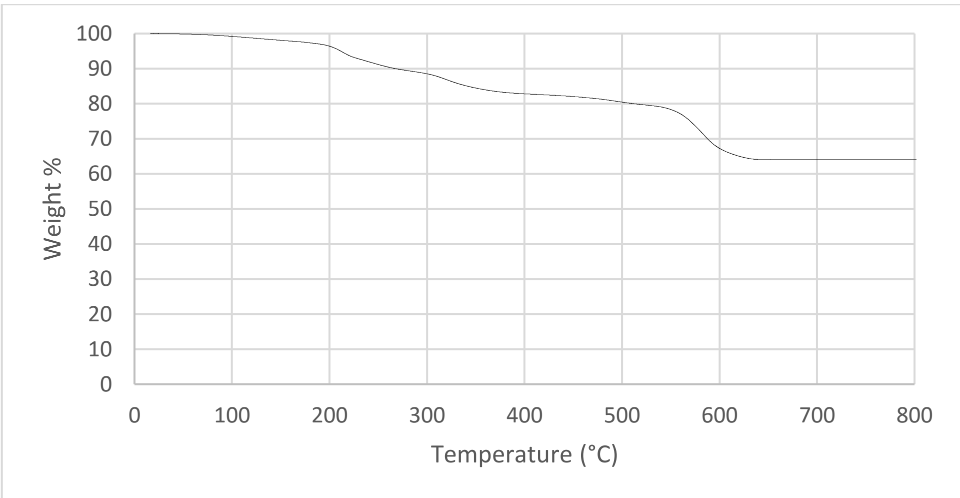

Figure S20. TGA analysis for compound **3** (recorded in N_2 atmosphere; heating rate 10 ^oC/min.)

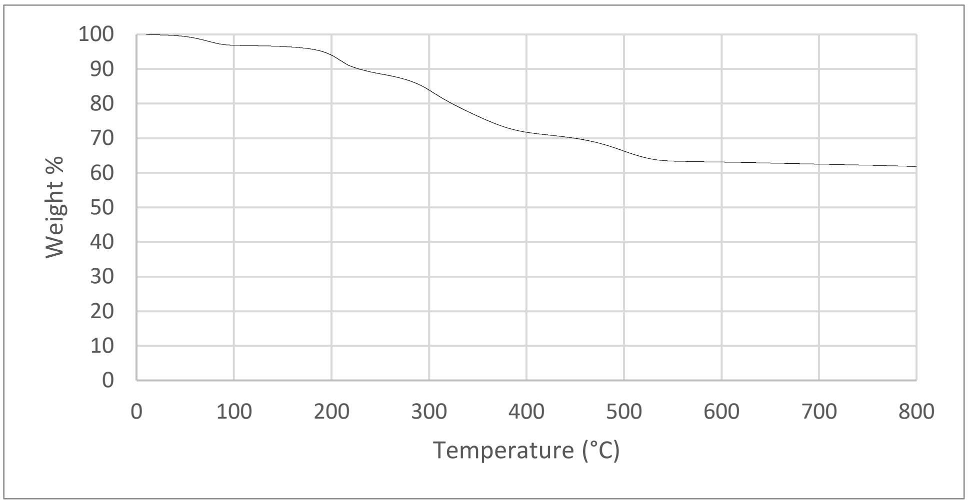

Figure S21. TGA analysis for compound **4** (recorded in N_2 atmosphere; heating rate 10 ^oC/min.)

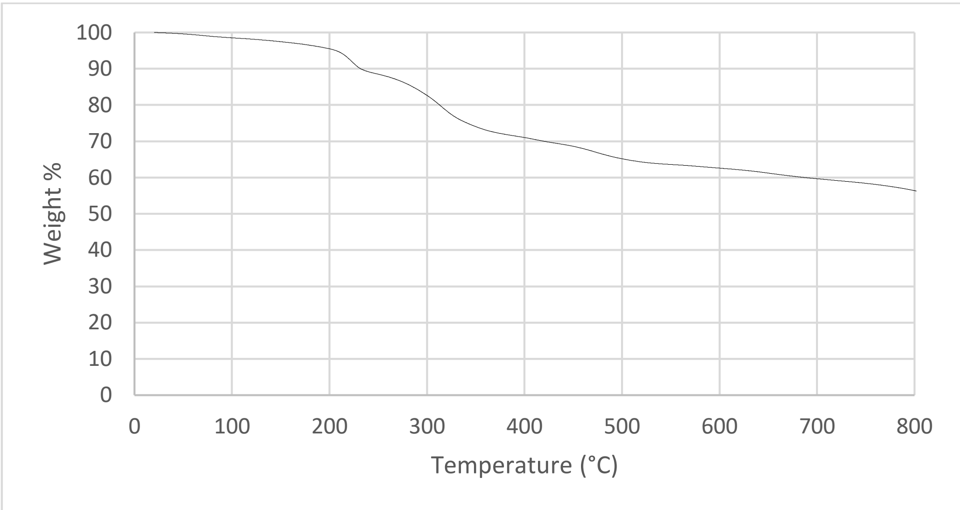

Figure S22. TGA analysis for compound **5** (recorded in N_2 atmosphere; heating rate 10 ^oC/min.)

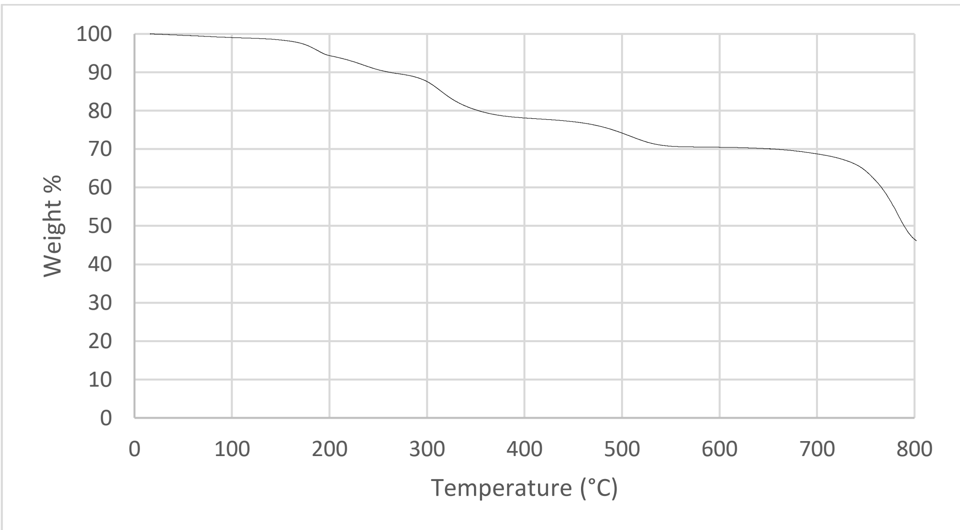

Figure S23. TGA analysis for compound **6** (recorded in N_2 atmosphere; heating rate 10 ^oC/min.)

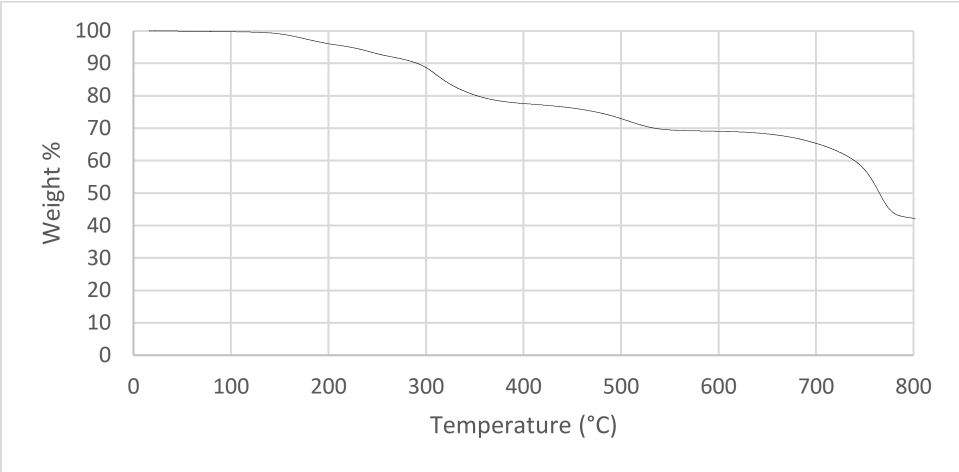

Figure S24. TGA analysis for compound **7** (recorded in N_2 atmosphere; heating rate 10° C/min.)

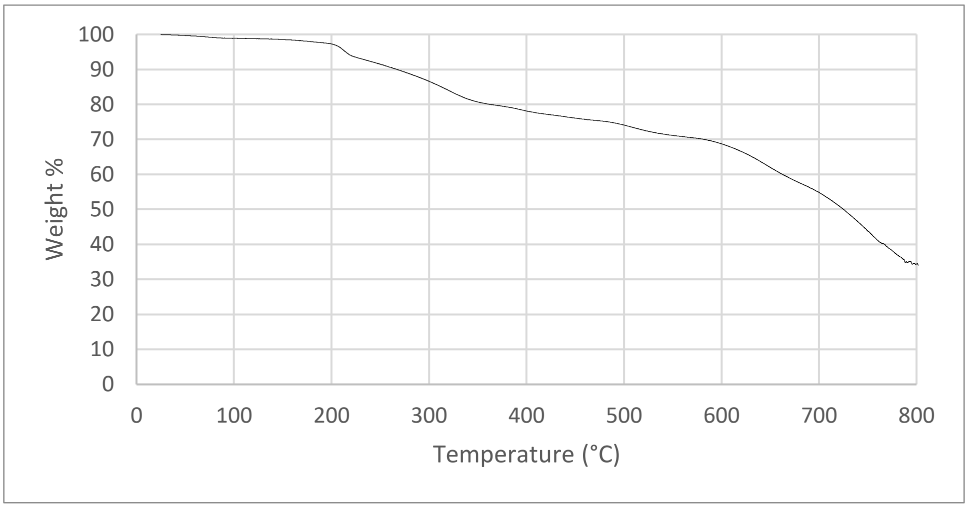

Figure S24. TGA analysis for compound **8** (recorded in N_2 atmosphere; heating rate 10 °C/min.)

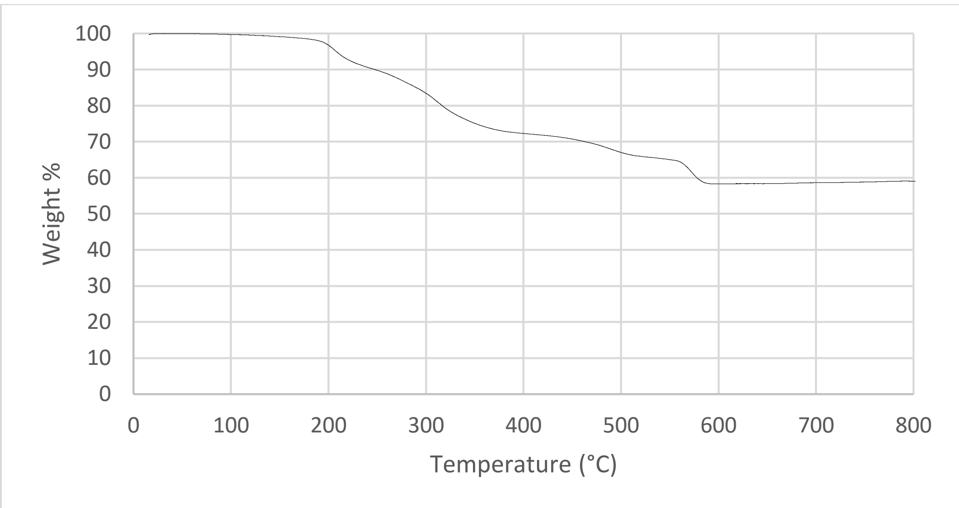

Figure S25. TGA analysis for compound **9** (recorded in N_2 atmosphere; heating rate 10 °C/min.)

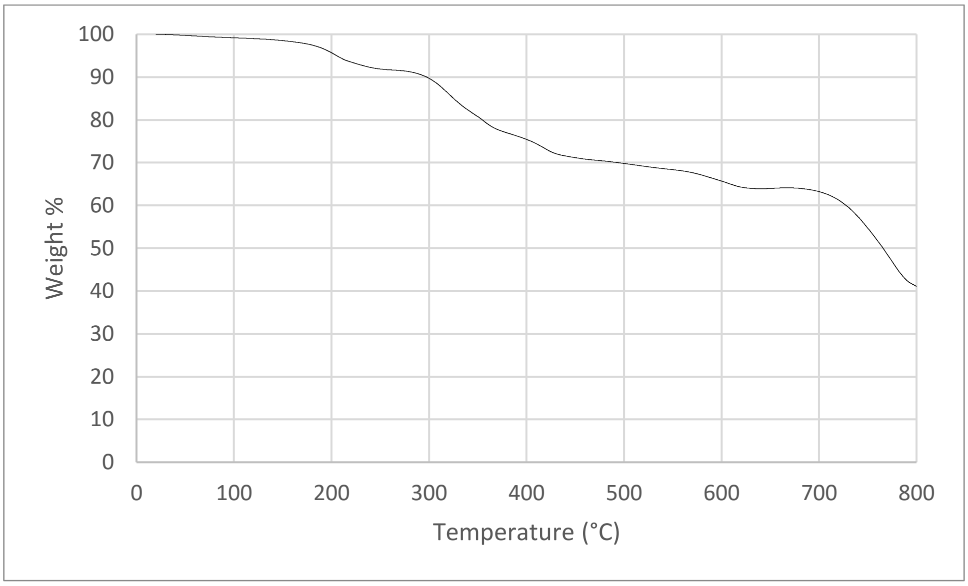

Figure S26. TGA analysis for compound **10** (recorded in N_2 atmosphere; heating rate 10 ^{o}C/min.)

11) Unidentified Powder Material

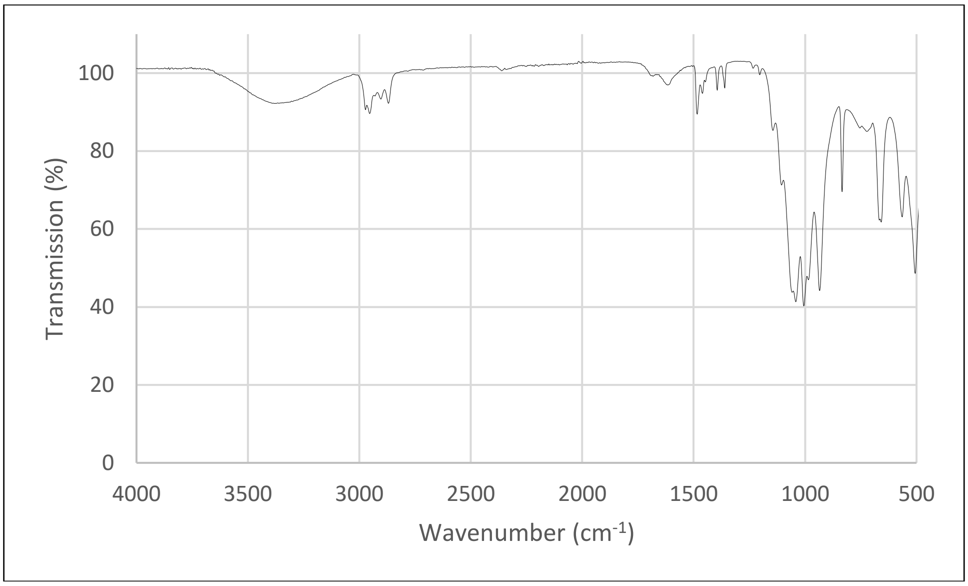

Figure S27. IR spectrum for the unidentified blue material obtained from substituting sodium molybdate, Na_2MoO_4, into the synthesis of **1** in place of Lindqvist hexamolybdate, $(TBA)_2(Mo_6O_{19})$. Presence of strong bands at around 1000 cm^{-1} are assigned as phosphonate (P-O) stretching features.

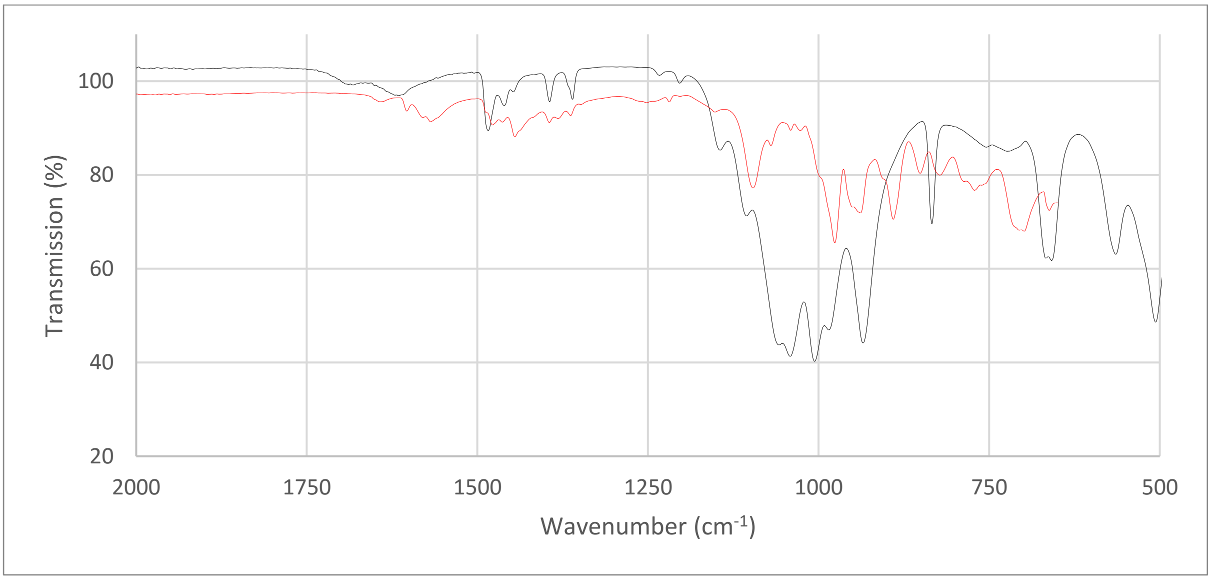

Figure S28. Comparison of the IR spectrum for the unidentified blue material (black) compared to the IR spectrum for **1** (red). Although the blue material has not been fully characterised, it is demonstrably different from compound **1**, supporting our hypothesis that compound **1** can only form from fragments generated by top-down disassembly processes.

12) References

1 N. J. Hur, W. G. Klemperer and R. C. Wang, Inorg. Synth., 1990, 27, 77.
2 P. C. Crofts and G. M. Kosolapoff, J. Am. Chem. Soc., 1953, 75, 3379.
3 M. E. Fleet, Miner. Mag., 1976, 40, 531.
4 M. Wildner, Z. Krist., 1992, 202, 51.
5 M. Hughes, F. Foit and E. Wright, Can. Mineral., 2002, 40, 153.
6 L. Yang, D. R. Powell and R. P. Houser, Dalton Trans., 2007, 955.
7 A. W. Addison and T. N. Rao, J. Chem. Soc. Dalt. Trans., 1984, 1349.